POLITECNICO DI MILANO
School of Industrial and Information Engineering
Master's Degree in Space Engineering
Department of Aerospace Science and Technology

Proximity trajectory design for a CubeSat around binary asteroid Didymos

Supervisor : Prof. Francesco Topputo
Coadvisor : Dr. Fabio Ferrari

Candidate:
Claudio Bottiglieri
Matr: 914472

Academic Year 2019-2020

Alle persone che amo e che mi amano. Perchè nella vita, nulla è importante, se non la condividi con loro.

Acknowledgments

At the end of the toughest year my generation has faced, I am about to finish my Master's thesis and take the last step to fully enter adulthood. When everything in life is made so uncertain by events greater than you, you understand the importance of making sense of what you do. For this, it becomes necessary to thank some people without whom I would not have become the man and now the engineer I am.

First, I would like to thank my Professor, Francesco Topputo. The professional and friendly environment that he creates around himself has brought out the best in me, always making me feel at ease. His trust was the fuel needed to stimulate me without letting me rest on that. However, this project would not have been completed without the support of Doctor Fabio Ferrari. His punctual and never sticky presence was essential to ensure the necessary technical, but above all emotional, support.

Special thanks go to my family. To my mother whose rigor has taught me that what matters must be conquered with sacrifice and diligence. To my father, I became a man by learning from you the importance of always questioning myself and not being afraid of my fragility. Thanks to my brother Valerio and my granparents whose wisdom taught me the importance of education.

Thanks to my mentor, Chiara. You have guided me through this jungle called Engineering. A world of thanks to my second family, the unique 5D. Although distant, our hearts will always beat all together.

No special words are needed to my non-blood brother, Mario. Together we have faced and continue to face the greatest challenge of all: life.
Thanks Claudia. I have always felt you by my side. Although your anger is one of the things I fear most in the world, your charges has given me so much and made me who I am now. Without you, I wouldn't have gotten very far. Thank you.

I own infinite gratitude to my spiritual guide, Federica and to Roberto and Alessandra. You are the family I choose to have.

I am what I am also thanks to Costanza, Gabriele, Michele, Francesco (Punzo) and Paolo. Thanks.

Thanks Paola, Raffaello and Giovanni, you have always welcomed me as a part of your family.

Finally, I owe more than a thank you to Francesca. We met just in time to face this path together, hand in hand. I am glad for the day we met, which was early enough to grow up together and mature enough to understand the gift we have received. And I thank you for all the love you have given me over the years. You have donated me the happiness that allowed me to endure the tough challenges of this journey with a smile on my face. This year has been characterized by one depression after another, but I could not have dealt with it without you. Indeed, you were the only positive note of all the sacrifices caused by the Corona. Thank you.

Abstract

The investigation of small bodies through proximity operations and landing is the future of the current space exploration. Achieving these goals with low-cost solutions as CubeSats can be the required boost to accelerate the European race for space. The present work is a step forward a more extensive use of CubeSats for deep space exploration. Through a characterization of the dynamical environment around Didymos, a Near Earth binary Asteroid, the thesis aims to find proximity trajectories around it for a CubeSat. Orbiting around asteroids can be challenging due to their irregular gravity field generated by their complex mass distribution. In the past, different gravity models have been used to design the gravity field around small bodies. Spherical harmonics and complex shape-based models have been investigated in this work with the aim of finding the best representation of the gravity field close to the asteroid. Additional complexity is given by the inherent non-Keplerian dynamics around a binary system which precludes any analytical solutions, a complex scenario in which mission designers have to work. However, non-Keperlian problems can offer advantageous trajectories precluded to a simple two body problem and for this reason they are one of the main current interests of the scientific community. This issue has been addressed in this thesis by working in a high fidelity model considering a generic restricted three body problem. After the characterization of the dynamical system, close trajectories have been designed and reproduced to obtain possible solutions for future observation strategies. From the results, some important information and features have been extrapolated as possible trajectories design strategies for future works.

Keywords: CubeSats; Binary Asteroid; Restricted Three Body Problem; Trajectory Design; Gravitational Model; Proximity Operations;

Sommario

Lo studio dei corpi minori attraverso operazioni di prossimità e tentativi di atterraggi è il futuro dell'attuale esplorazione spaziale. Raggiungere questi obbiettivi con soluzioni a basso costo come i CubeSats può essere la spinta necessaria per accelerare la corsa Europea allo spazio. Il seguente lavoro è un ulteriore passo verso un uso maggiore dei CubeSats per l'esplorazione dello spazio profondo. Attraverso una caratterizzazione dell'ambiente dinamico vicino Didymos, un asteroide binario orbitante vicino alla Terra, la presente tesi si prefissa di trovare traiettorie ad esso ravvicinate per un CubeSat. Orbitare attorno ad asteroidi può essere impegnativo a causa del loro campo gravitazionale irregolare generato dalla loro forma complessa. Diversi modelli sono stati usati in passato per descrivere il campo gravitazionale attorno ai corpi minori. L'uso di modelli con forme complesse e armoniche sferiche è stato considerato in questo lavoro allo scopo di trovare la migliore rappresentazione del campo gravitazionale prossimo all'asteroide. Ulteriore difficoltà è data dal problema non kepleriano attorno a un sistema binario che preclude l'esistenza di qualsiasi soluzione analitica, uno scenario complesso in cui gli ingegneri di volo devono lavorare. Tuttavia, problemi non kepleriani possono offrire traiettorie vantaggiose precluse a un semplice problema a due corpi e per questo sono uno degli interessi attuali della comunità scientifica. Al termine di una caratterizzazione del sistema dinamico, traiettorie di prossimità sono state progettate e simulate al fine di ottenere possibili soluzioni per future strategie di osservazione. Dai risultati, importanti informazioni e caratteristiche sono state estrapolate come possibili strategie di progettazione di traiettorie per lavori futuri.

Parole chiave: CubeSats; Asteroidi Binari; Problema Ristretto a Tre Corpi; Progettazione di Traiettoria; Modelli Gravitazionali; Operazioni di Prossimità;

Contents

List of Figures

List of Tables

Chapter 1

Introduction

Over the past twenty years, space exploration has vastly expanded its horizons by introducing a new concept of satellites that greatly reduces manufacturing costs, CubeSats. This has not only opened the space sector to low-budget companies, but has also made agencies more prone to high-risk operations, opening a huge window of new missions opportunities. Due to their relatively fast development, it is now mandatory to study CubeSats' actual capabilities or limitations away from Earth.
Concurrently, the first rendezvous missions targeting asteroids began. As for CubeSats, asteroids represent a huge opportunity for space exploration, since they carry with them important information about the solar system and the life origin. In addition, a population of them, the Near Earth Asteroid (NEA), has opened the possibilities of a large number of scientific missions targeting bodies that can be reached easier than the Moon. Moreover, some of them intersect the Earth's orbit, and for that, are also being investigated for planetary defence purpose. However, operating around small bodies is not as easy as it is for planets due to their weak and irregular gravity field. Different strategies have been used in the past to address these irregularities. Shape-based models can be adopted to reproduce the gravity field of homogeneous bodies once their shape and density are known. Conversely, mass-concentrated models can be used to represent bodies with voids and irregularities in the density distribution, as long as these information is provided or assumed.
Additional complexity is present if the target is a binary asteroid. As a high risk-high reward mission, targeting a binary asteroid can be productive since their mass and density can be easily retrieved, but also troublesome, since having more than one gravitational source with comparable mass leads to non-Keplerian dynamics which is a matter hard to deal with. No general analytical solution is present and numerical methods are the only way to find particular trajectories close to such binary systems. However, although relevant solutions have been found for a three-body problem in the form of periodic orbits and

trajectories close to the Lagrangian points, the general three body problem is still far to be considered as fully understood.
Yet, non-Keplerian dynamics can offer new and low-cost transfer solutions along with proximity trajectories forbidden in a simple two body problem and this is why it is a current interest for new millennium space mission designers.

1.1 Historical review

Asteroids are small bodies orbiting the Sun primarily between Mars and Jupiter in what it is known as Main Belt. Due to the large amount of information they possess on planets and the origin of life, they have always represented a theme of great scientific interest in space exploration. Indeed, the first mission targeting a small body dates to 1996 when NASA's Near Earth Asteroid Rendezvous (NEAR-Shoemaker) concluded the first non-incidental close rendezvous with an asteroid, (253) Mathilde, in 1997. NEAR-Shoemaker achieved also the first soft-landing on (433) Eros' surface in 2001[1].
Close rendezvous and landing are non trivial activities for spacecrafts dealing with bodies characterized by strongly irregular mass distributions and so irregular gravity fields. Therefore, in order to perform invaluable operations around small bodies, it is necessary to efficiently overcome the technological challenges that they entail by implementing innovative solutions.
One of the biggest challenges posed by close operations to asteroids is radio communication with the ground and its drawbacks in terms of speed and accuracy. Many has thought of overcoming this limit by directly eliminating ground control, introducing degrees of autonomy in operations. This would bring a huge benefit also from the economical point of view in terms of less resources usage. However, NASA is also planning to increase communication performances of spacecrafts with the use of lasers instead of radio waves. In 2026, the mission Psyche is going to communicate with Earth in optical frequency with a huge planned benefit in terms of efficiency without worsen the mass, volume or power demands[2][3]. NASA has already demonstrated the performance of optical communication in the Lunar Atmosphere and Dust Environment Explorer (LADEE) mission[4] and now it is going to use it targeting the metal asteroid (16) Psyche.

NEA - A scientific interest and a technology demonstration occasion

In recent years, many missions have followed the trend of autonomous operations, especially around Near-Earth Asteroids (NEA), small bodies with semi-major axis of about 1 AU. Due to their large accessibility to spacecrafts, NEAs are the current frontier for small bodies exploration. A recent rendezvous with a NEA and the first sample return mission is Hayabusa by the

Japan Aerospace eXploration Agency (JAXA) in 2005[5][6].
Hayabusa collected a small sample from the surface of Itokawa performing a so called touch-and-go procedure where the spacecraft descents near the surface for the time necessary to collect samples and lifts off before being damaged. Such critical and hazardous operations require the presence of an accurate and autonomous control since ground control would be slow and inaccurate. The cancellation of horizontal velocity and the safety maneuver after the sample collection are two of the most important operations to be controlled on board. In particular, Hayabusa kept track of an artificial landmark on the surface to check for its relative position with respect to the sampling site. Landmark navigation uses targets onto the surface (natural or placed artificially) to orient the spacecraft motion working as points of reference for the navigation. This, allowed Hayabusa for hoovering on the surface during the sampling procedure. The mission was so successful that it was followed by its evolution, Hayabusa 2[7]. Hayabusa 2 is a more massive, redundant and with higher scientific capability version of Hayabusa. It is expected to return in December 2020 with three sampling from 1999JU3 obtained with the same touch-and-go procedure of Hayabusa. This time, five spherical artificial markers of a diameter of 100mm were used to estimate the position.
Although it was not provided with any autonomous navigation features, Rosetta [8][9] is worth of mentioning among the missions targeting small bodies. As the first rendezvous with a comet achieved in 2014, Rosetta was the first time that optical navigation with landmark was used in ESA operations.
Nowadays, landmarks navigation can be performed in a completely autonomous way as seen recently during OSIRIS REx close operations.
OSIRIS REx is a sample return mission to asteroid Bennu, actually operating and performing close proximity functions, planned to end in 2023 [10][11][12]. Its sample recovery strategy is similar to Hayabusa, performing a touch-and-go landing, while the close proximity navigation is fully autonomous exploiting a natural target tracking strategy. Good accuracy is guaranteed since, after a detailed survey campaign, enough information has been provided to build a 3D model of the asteroid's shape.
Moving towards fully autonomous operations there is M-ARGO[14]. Miniaturised – Asteroid Remote Geophysical Observer, or M-ARGO, will be ESA's first stand-alone CubeSat for deep space targeting an asteroid. The mission has just completed its phase A of its developing, but the idea is to reach the target with a completely autonomous optical navigation during the approach phase. Proximity operations are dedicated to building a 3D model of the asteroid and navigating close to it using landmarks as tracking elements while hovering over the surface.

NEA crossing Earth - A planetary defense theme

Among NEAs there are also asteroids crossing Earth's orbit. Consequently, such asteroids represent a planetary defense theme which had inspired missions facing this problem like the Asteroid Redirect Mission (ARM)[13], now cancelled, NEA Scout[15] or the Asteroid Impact and Deflection Assessment (AIDA) mission[16].
The Near-Earth Asteroid Scout (NEA Scout) will be one of the thirteen CubeSats carried as secondary payload of the NASA mission Artemis 1 planned for the end of 2021. The official target is still unknown, but the mission's goal will be demonstrating the capability of reaching an asteroid proximity with a solar sail propulsion on a CubeSat.
Instead, AIDA is a joint mission between ESA and NASA aimed to demonstrate the kinetic impactor technique for planetary defense[16][17]. A NASA spacecraft, DART, will impact the moon of Didymos, a binary asteroid, while Hera, from ESA, will investigate the effect of such impact. Hera will be the first in-depth investigation of a binary asteroid. It will be equipped with a sensor suite consisting of optical cameras, a laser altimeter and a hyper-spectral imager which will guarantee complete autonomy during close proximity operations. Once in vicinity of the asteroid, two CubeSats will be released by Hera. The first, Juventas, is a 6U CubeSat responsible of observing the moon of the system from few km, while operating fully autonomously using the Hera mothercraft as a proxy[18].
The design for the second CubeSat has changed many times over the past years. The first concept was known as Asteroid SPECTral imaging mission (ASPECT) which was a 3U CubeSat demonstration mission with the goal of proving whether a CubeSat can handle operations in the rough environment close to a binary asteroid[19]. In addition, ASPECT should also have contributed from the scientific point of view by providing information on the composition of the asteroid's surface. ASPECT then evolved into APEX[20] which was a bigger CubeSat of 6U with more scientific instrument on-board. Recently, an ultimate project for the second CubeSat is born in September 2020 with the name of Milani. As for the previous ideas, Milani will navigate with the same degree of autonomy of Juventas exploiting its inner-satellite link radio with which it will be in contact with Hera[21].
The reason why AIDA's target was chosen is not only related to planetary defense. In fact, Didymos is a binary asteroid. Binary asteroids are the 16%[22] of NEA and they represent a strategic target for space exploration. Binary systems are characterized by two small bodies that are gravitationally bound and orbit around their common center of mass. Usually they are made of a bigger asteroid called primary and a smaller satellite called secondary. Something can be said about their formation although there is still a controversial debate

about it. Both bodies are believed to belong to the same original asteroid and their formation can be attributed to a collision for big systems with slow spin primaries, or to a fission due to an excessive spin rate for small systems with fast spin primaries. Since they enable investigation of properties that are often difficult to probe by other means, binary asteroids can be considered one of the most interesting population of NEA.

1.2 Motivation

During the space exploration of the last century, spacecrafts were large and unique vehicles characterized by a huge cost which allowed only few national agencies to launch them. However, in the new millennium, miniaturized satellites, the so called CubeSats, have captured the interest of the scientific community. Born as educational tools, they have began valuable low-cost solutions becoming the subjects of a large number of missions[2][14][18]. For this reason, it is crucial to investigate CubeSats' capabilities and limitations when operating in rough environments far from Earth.
The mission Hera involves the use of two CubeSats around the Near Earth Asteroid (NEA) Didymos and can be the perfect scenario to explore the dynamical solutions offered by miniaturized satellites. It is well known that NEAs represent a current theme for space exploration due to their proximity to Earth (1AU) and their threat as possible collider, so they have already been the target of many past missions. However, no satellite has ever achieved close exploration of a binary asteroid like Didymos. Considering the scientific opportunities offered by a binary asteroid and the uniqueness of a first in-depth mission around this type of asteroid, exploring the dynamical solutions offered by a CubeSat around Didymos can be both revealing and cutting edge.
Furthermore, the dynamical environment offered by a binary asteroid represents an additional benchmark for CubeSats. The weak and irregular gravity field of a small body and the three-body problem posed by a binary asteroid and the spacecraft lead to complex and non-Keplerian solutions. Orbiting around binary asteroids, especially in proximity where the irregularities play a major role in the dynamics, can be a challenging aspect to investigate. For this reason, the aim of this work is exploring the dynamical solutions in proximity of a binary asteroid to further contribute to the investigation of CubeSats' possibilities for deep space exploration.

1.3 Research question and objectives

The aim of this work is to study realistic dynamics of a CubeSat orbiting a binary asteroid like Didymos using a high fidelity model. However, the adopted strategy, as well as the knowledge obtained, can be easily adapted at any three-body system with strong irregularity in the gravity field. In brief, the main question that this thesis wants to answer is:
"*What are the actual capabilities of a CubeSat near a binary asteroid and what kind of solutions can be obtained?*
Then, the main research question is broken into three objectives of study, which are:

- Study the dynamical environment around the binary asteroid in a high fidelity model. The aim is to examine the forces acting on the third body and the order of magnitude of the perturbations. Therefore, the work intends to answer the question:
  "*How is the dynamical environment for a third body orbiting in proximity of the asteroid?*"

- Compare different strategies for the design of the irregular gravity field of the asteroid. From the comparison, it is possible to find the minimum distance at which the point-like model for the gravity field of the asteroid is reliable. Thus, the work intends to answer the question:
  "*Which is the best model for the gravity field close to the asteroid?*"

- Investigate particular solutions in proximity of the asteroid. The final purpose is to find possible non-trivial stable trajectories in the region between 4 and 10km from the binary system barycenter, and, if possible, orbits that are at a distance below 4km. These trajectories can be considered as a possible scenario for a close observation mission of the asteroid. Therefore, the work intends to answer the question:
  "*What are the operative regions in which close trajectories can be obtained around the asteroid?*".

1.4 Thesis overview

This work mainly deals with the analysis of the dynamical environment around a binary asteroid and the possible close solutions around it. The results can be considered as possible observation trajectories around Didymos, the case study.
After this short introductory chapter, Chapter 2 will be about the background knowledge on the problem's dynamic. The Non-Keplerian environment, the equations of motion and the involved dynamical elements are described.
Chapter 3 describes the model of the dynamical environment considered, together with its validation.
Chapter 4 is about the software architecture used for the propagation of proximity orbits.
In Chapter 5 the results are shown and Chapter 6 summarizes all the work and shows the results inherent to the presented research questions.

Chapter 2

Theoretical Background

The general solution to the orbital problem around a binary asteroid is one of the most challenging aspect of operating around them, since it requires: the solution of the mutual orbital and rotational motion of the bodies, the modelling of their non-spherical mass distribution and the not negligible Sun perturbation on the system. In this section, the background knowledge about the dynamical problem under investigation is present. The Non-Keperlian dynamical environment generated by multiple bodies is mentioned and the decrescent hierarchical order of models is shown down to the RF3BP adopted in this work. The equations of motion and the main dynamical elements are shown together with the perturbations considered.

2.1 Non-Keplerian dynamical models

General problem

The general formulation of the problem of a mass-less particle orbiting a binary asteroid orbiting the Sun is a Restricted Hill Full Four Body Problem (RHF4BP). "Restricted" due to the negligible mass of the spacecraft, "Hill" as the asteroids and the spacecraft are relative close to each other in orbit around a more massive body and "Full" due to the non-spherical mass distribution of the asteroids. Scheeres and Bellerose[23] derived the equations of motion for this problem by considering the case of a spacecraft orbiting a binary asteroid. However, to solve for the spacecraft, it is necessary to first have dealt with the motion of the primaries (asteroids and Sun) in what can be considered a Hill Full 3 Body problem. Although the HF3BP has been extensively studied in the past[24], it is evident that this problem is complex to be handled and it may be convenient to consider the Sun as a perturbation, and the solution of particle motion as a Restricted Full Three Body Problem (RF3BP) around asteroids. Consequently, the asteroids' motion can be studied as a F2BP.

Full 2 Body Problem F2BP

The Full Two Body Problem studies the motion of two bodies with comparable mass and non-spherical shape under the influence of their mutual attraction. The general formulation of the F2BP can be troublesome due to its 12 degrees of freedom and the coupling between the translation and rotational motion introduced by the non-spherical mass distribution. Several results have been obtained by assuming at least one body spherical [25] or assuming the bodies as polyhedra[26].Scheeres has studied the stability of the problem in case both bodies are non spherical, but considering planar motion[27]. For simplicity, the formulation found in [23] is reported here for a complete description of the problem. The model used is a sphere-approximation for one of the asteroids and the dimensionsless equations of motion in Eq. (2.1) are derived in a body fixed frame centered in the barycenter of the binary system. As it can be seen in the equations, the advantage of considering a spherical approximation is to decouple the rotational dynamics of that body from the system.

$$\ddot{\mathbf{r}}_B + 2\omega \wedge \dot{\mathbf{r}}_B + \dot{\omega} \wedge \mathbf{r}_B + \omega \wedge (\omega \wedge \mathbf{r}_B) = \frac{\partial \tilde{U}}{\partial \mathbf{r}_B} \tag{2.1}$$

$$\mathbf{I} \wedge \dot{\omega} + \omega \wedge \mathbf{I}\omega = -\nu \mathbf{r}_B \wedge \frac{\partial \tilde{U}}{\partial \mathbf{r}_B} \tag{2.2}$$

Here, $\mathbf{r}_B$ is the relative position vector between the two mass centers, the time derivatives are considered as taken in the body-fixed reference frame and ω is the angular velocity of the general body, $\mathbf{I}$ is its inertia matrix normalized by the mass, ν is:

$$\nu = \frac{M_1}{M_1 + M_2}$$

$\tilde{U}$ is the mutual potential defined as:

$$\tilde{U} = \frac{\alpha}{M_2} \int_{B2} \frac{dm_2(\rho)}{|\mathbf{r}_B + \rho|} \tag{2.3}$$

where ρ is the position vector of the infinitesimal mass dm_2.
All the dimensional parameters are normalized by the maximum radius of the distributed body α and the mean motion of the system at that radius.
In this work, solving the motion of the asteroids was not necessary since their ephemerides were taken from ESA database*.

*https://www.cosmos.esa.int/web/spice/spice-for-hera

Restricted Three Body Problem R3BP

The Restricted Three Body Problem studies the motion of a particle, which moves under the attraction of two massive bodies, the primaries. Depending on the motion of the primaries, this problem has been extensively studied considered as a Circular Restricted Three Body Problem (CR3BP) or Elliptical Restricted Three Body Problem (ER3BP). In this work, the goal was to describe the dynamical environment with a high fidelity model and therefore the following formulation is based on a generic R3BP.

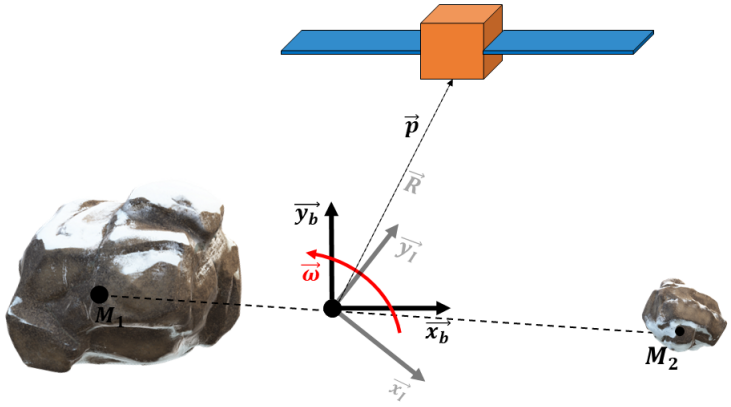

Figure 2.1: The Restricted Three Body Problem formed by the mass-less spacecraft and the two asteroids. In grey, the inertial reference frame, in black the body-fixed reference frame.

Once the dynamical background has been properly introduced, the equations of motion can be written. To obtain them, a newtonian approach was used and the dynamics can be expressed in an inertial reference frame as in Eq. (2.4):

$$\ddot{\mathbf{R}} = \frac{\partial U_1}{\partial \mathbf{R}_1} + \frac{\partial U_2}{\partial \mathbf{R}_2} \tag{2.4}$$

where U_1 and U_2 are the gravitational potentials of the primaries, $\mathbf{R}$ is the position of the third body with respect to the barycenter of the binary system and $\mathbf{R}_1$ and $\mathbf{R}_2$ are the relative positions of the third body with respect to the asteroids. The acceleration can be additionally enriched by adding the perturbations considered, as the SRP described in Section 2.4. Once the potential has been modelled, the problem can be entirely treated using Eq. (2.4) since the positions of the primaries are assumed to be known. However, it may be convenient to express the equations in terms of a body fixed frame in which the gravity potential of the asteroids can be considered time invariant and can be easily computed as shown in Section 2.2.

As graphically shown in Fig. 2.1, the body fixed reference frame considered is centered in the system barycenter and its axis are parallel to the principal axis of the primary asteroid. Assuming the inertial z-axis coincident with the body's one, the rotation of the asteroid only influences the relative position of the x an y components. Consequently, to convert the position of the spacecraft in the body fixed frame, a planar rotation of the xy plane around z is necessary and obtained through the matrix $\mathbf{T}$ as seen in Eq. (2.5) and Eq. (2.6).

$$\mathbf{p}(t) = \mathbf{T}(\omega, t)\mathbf{R}(t) \tag{2.5}$$

$$\mathbf{T}(\omega, t) = \begin{bmatrix} \cos\omega t & \sin\omega t & 0 \\ -\sin\omega t & \cos\omega t & 0 \\ 0 & 0 & 1 \end{bmatrix} \tag{2.6}$$

The rotation matrix $\mathbf{T}$ is orthonormal. Thus, the inertial position of the third body can be written as in Eq. (2.7).

$$\mathbf{R}(t) = \mathbf{T}(\omega, t)^\top \mathbf{p}(t) \tag{2.7}$$

Therefore, the acceleration in the inertial frame can be rewritten as in Eq. (2.8).

$$\begin{aligned} \ddot{\mathbf{p}}(t) &= (\ddot{\mathbf{T}}(\omega, t)^\top \mathbf{p}(t)) \\ &= \ddot{\mathbf{T}}(\omega, t)^\top \mathbf{p}(t) + 2\dot{\mathbf{T}}(\omega, t)^\top \dot{\mathbf{p}}(t) + \mathbf{T}(\omega, t)^\top \ddot{\mathbf{p}}(t) \end{aligned} \tag{2.8}$$

By substituting Eq. (2.8) into Eq. (2.4) and by rotating the right hand side, Eq. (2.9) is obtained.

$$\ddot{\mathbf{T}}(\omega, t)^\top \mathbf{p}(t) + 2\dot{\mathbf{T}}(\omega, t)^\top \dot{\mathbf{p}}(t) + \mathbf{T}(\omega, t)^\top \ddot{\mathbf{p}}(t) = \mathbf{T}(\omega, t)^\top \left(\frac{\partial U_1}{\partial \mathbf{p}_1} + \frac{\partial U_2}{\partial \mathbf{p}_2} \right) \tag{2.9}$$

By pre-multiplying each quantity per $\mathbf{T}$ and considering that:

$$\mathbf{T}(\omega, t) \cdot \mathbf{T}(\omega, t)^\top = \mathbf{I}$$

$$\mathbf{T}(\omega, t) \cdot \dot{\mathbf{T}}(\omega, t)^\top = \begin{bmatrix} 0 & -\omega & 0 \\ \omega & 0 & 0 \\ 0 & 0 & 0 \end{bmatrix}$$

$$\mathbf{T}(\omega, t) \cdot \ddot{\mathbf{T}}(\omega, t)^\top = -\omega^2 \mathbf{I}$$

the equations of motion in the body frame can be written as in Eq. (2.10)

$$\ddot{\mathbf{p}} + 2\omega \wedge \dot{\mathbf{p}} + \omega \wedge (\omega \wedge \mathbf{p}) = \frac{\partial U_1}{\partial \mathbf{p}_1} + \frac{\partial U_2}{\partial \mathbf{p}_2} \tag{2.10}$$

where $\mathbf{p}$ is the position of the particle and ω is the angular velocity of the asteroid around its axis.

2.2 Small bodies gravitational models

The distinguished features of small bodies are their irregular shapes and hence their strong non-spherical mass distribution. This peculiarity leads to a complex evaluation of the gravity potential generically expressed as:

$$U(\mathbf{r}) = G \int_B \frac{dm(\rho)}{|\mathbf{r} - \rho|} \tag{2.11}$$

To easily deal with this quantity, a common strategy used for planets is to consider a spherical model. The irregularities are then accounted with the addition of harmonic expansions of the gravitational potential. For this purpose, spherical or ellipsoidal harmonics have been both used in past.[28]. These methods exploit the separation of variables in terms of spherical coordinates and then the transition from the integral to a Laplace series expansion. As a drawback, these methods work well with planets which are quasi-spherical bodies since the convergence of the series to the actual field is ensured up to the Brillouin sphere, the sphere circumscribing the body. With elongated and complex shape bodies, as asteroids or comets, it is hard to design proximity operations that do not enter this boundary.

Figure 2.2: Brillouin sphere around an asteroid. The divergence zone is highlighted in red.

A better choice for complex shapes would be to consider exact solutions coming from definite shape like a polyhedron or an ellipsoid. In this way, no regions of divergence are present since the solution is exact. The problem of these formulations relies on the fact that the body's shape can be different with respect to the best model that can be used, introducing an error.

Spherical harmonics

The most common harmonic expansion is the one using spherical harmonics. As seen in [29], the gravitational potential can be expressed as an infinite series

as shown in Eq. (2.12).

$$U(r,\delta,\lambda) = \frac{\mu}{r}\sum_{l=0}^{\infty}\sum_{m=0}^{l}\left(\frac{R_0}{r}\right)^l P_{lm}(\sin\delta)[C_{lm}\cos m\lambda + S_{lm}\sin m\lambda] \tag{2.12}$$

$$\begin{cases} r = \sqrt{x^2+y^2+z^2} \\ \sin\delta = \frac{z}{r} \\ \tan\lambda = \frac{y}{x} \end{cases}$$

Therefore, the problem is shifted to the evaluation of the polynomial coefficients. It can be shown that there is a relationship between the gravity coefficients of all degree and orders and the high-order mass distribution moments of the body.
By performing the gradient of the potential, the contribution to the acceleration can be derived as seen in [29] obtaining Eq. (2.13).

$$\mathbf{a} = -\frac{GM}{R^2}\hat{\mathbf{r}} + \sum_{l=1}^{\infty}\sum_{m=0}^{l}\mathbf{a}_{l,m} \tag{2.13}$$

$$\begin{aligned}\mathbf{a}_{l,m} =& \frac{GMR_0^l}{R^{l+m+1}}\Bigg\{\frac{C_{l,m}C_m + S_{l,m}S_m}{R}[A_{l,m+1}\hat{\mathbf{e}}_3 - (\sin\delta A_{l,m+1} + (l+m+1)A_{l,m}\hat{\mathbf{R}}]+ \\ & mA_{l,m}[(C_{l,m}C_{m-1} + S_{l,m}S_{m-1})\hat{\mathbf{e}}_1 + (S_{l,m}C_{m-1} - C_{l,m}S_{m-1})\hat{\mathbf{e}}_2]\Bigg\}\end{aligned}$$

Here, R is the position vector of the field point, R_0 is an arbitrary reference radius of the body, $C_{l,m}$ and $S_{l,m}$ are the spherical harmonics coefficients, while $\hat{\mathbf{e}}_1$, $\hat{\mathbf{e}}_2$ and $\hat{\mathbf{e}}_3$ are three unit vector mutually perpendicular fixed to the body. They are usually the axis of a body fixed frame.
C_m and S_m are parameters related to the equatorial shape of the body. Defined in [30], they can be expressed as in Eq. (2.14)

$$S_m \triangleq \rho^m \sin m\lambda \qquad C_m \triangleq \rho^m \cos m\lambda \tag{2.14}$$

where:

$$\rho^2 \triangleq (\mathbf{R}\cdot\hat{\mathbf{e}}_1)^2 + (\mathbf{R}\cdot\hat{\mathbf{e}}_2)^2 \tag{2.15}$$

$A_{l,m}$ represents the derived Legendre polynomial of degree l and order m related to the associate Legendre function $P_{l,m}$ and can be obtained as in Eq. (2.16)

$$A_{l,m}(\sin\delta) = \left(\frac{R}{\rho}\right)^m P_{l,m}(\sin\delta) \tag{2.16}$$

For a complete description and the derivation of the acceleration gradient see [29].

Polyhedron shape

If a shape model is available, the best representation would be an homogeneous polyhedron with constant density. Despite the complexity, this strategy can be extremely powerful as it is able to give accurate modelling of complex shapes. As done for (216) Kleopatra, shown in Fig. 2.3.

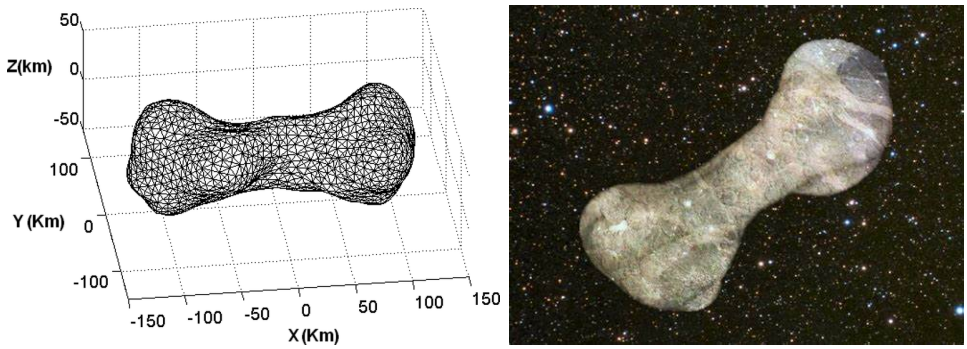

(a) **(b)**

Figure 2.3: (a) Polyhedron model 3D of asteroid (216) Kleopatra. The shape was built with 4092 faces. (b) Radar image of Kleopatra (Credit: Stephen Ostro et al. (JPL), Arecibo Radio Telescope, NSF, NASA), texture and colours are fake.

As shown by [33] in detail, the potential of a polyhedron can be expressed as:

$$U_{poly}(x,y,z) = -\frac{1}{2}G\rho\left(\sum_{f\in\text{Faces}} \mathbf{r}_f \cdot (\mathbf{F}_f \cdot \mathbf{r}_f)\,\omega_f - \sum_{e\in\text{Edges}} \mathbf{r}_e \cdot (\mathbf{E}_e \cdot \mathbf{r}_e)\,L_e\right) \tag{2.17}$$

This is an analytical expression that consider the sum of the potential of the faces and edges of the polyhedron.
The first contribution is made by the quadratic multiplication between $\mathbf{r}_f$, the vector from the field point to face f and the associated dyad $\mathbf{F}_f$ obtained from the dyadic product of the unitary vector normal to f, $\hat{\mathbf{n}}_f$, with itself.

$$\mathbf{F}_f = \hat{\mathbf{n}}_f \hat{\mathbf{n}}_f \tag{2.18}$$

Similarly, the second contribution is obtained considering the vector connecting the field point and the edge e, $\mathbf{r}_e$, and the dyad $\mathbf{E}_e$ obtained as follow:

$$\mathbf{E}_e = \hat{\mathbf{n}}_{f1}\hat{\mathbf{n}}_e^{f1} + \hat{\mathbf{n}}_{f2}\hat{\mathbf{n}}_e^{f2} \tag{2.19}$$

$\hat{\mathbf{n}}_e^{f1}$ is the unitary vector normal to the edge e and to $\hat{\mathbf{n}}_{f1}$ and pointing opposite with respect to the centre of face f_1. The same is valid for the face f_2.

Both contributions are then multiplied by a scalar parameter. ω_f multiplies the contribution of the faces and represents the solid angle of f seen by the field point, which is:

$$\omega_f = 2 \arctan \frac{\mathbf{r}_1^f \cdot \mathbf{r}_2^f \wedge \mathbf{r}_3^f}{r_1^f r_2^f r_3^f + r_1^f \mathbf{r}_2^f \cdot \mathbf{r}_3^f + r_2^f \mathbf{r}_1^f \cdot \mathbf{r}_2^f + r_3^f \mathbf{r}_1^f \cdot \mathbf{r}_2^f} \tag{2.20}$$

here, $\mathbf{r}_1^f$, $\mathbf{r}_2^f$ and $\mathbf{r}_3^f$ are the vectors connecting the field point to the vertexes of the triangular face
Differently, L_e represents the potential of a wire associated to the edge e which is:

$$L_e = \ln \frac{r_1^e + r_2^e + l^e}{r_1^e + r_2^e - l^e} \tag{2.21}$$

where r_1^e and r_2^e are the vectors connecting the field point to the vertexes at the end of edge e.
As the gradient of the potential expressed in Eq. (2.17), the acceleration can be computed as shown in Eq. (2.22)

$$\mathbf{a_{poly}} = G\rho \left(\sum_{f \in \text{Faces}} \mathbf{F}_f \cdot \mathbf{r}_f \omega_f - \sum_{e \in \text{Edges}} \mathbf{E}_e \cdot \mathbf{r}_e L_e \right) \tag{2.22}$$

By performing the second derivatives, the Jacobian che be then computed as in Eq. (2.23)

$$\nabla \mathbf{a}_{poly} = -G\rho \left(\sum_{f \in \text{Faces}} \mathbf{F}_f \omega_f - \sum_{e \in \text{Edges}} \mathbf{E}_e L_e \right) \tag{2.23}$$

Ellipsoidal shape

A simpler solution with respect to the polyhedron shape is to model the asteroid as a constant density ellipsoid with semi major axis $\gamma < \beta < \alpha$. Simpler than a polyhedron model, this strategy can be convenient for quasi-elliptical bodies as for Itokawa (Fig. 2.4)

As seen in [32] the potential for the ellipsoid can be expressed as:

$$U(r) = -\frac{3}{4}\mu \int_{\lambda(r)}^{\infty} \Phi(\mathbf{r}, u) \frac{du}{\Delta(u)} \tag{2.24}$$

where

$$\begin{cases} \Phi(\mathbf{r}, u) = \frac{x^2}{\alpha^2+u} + \frac{y^2}{\beta^2+u} + \frac{z^2}{\gamma^2+u} - 1 \\ \Delta(u) = \sqrt{(\alpha^2+u)(\beta^2+u)(\gamma^2+u)} \\ \lambda \quad | \quad \Phi(\mathbf{r}, \lambda) = 0 \end{cases} \tag{2.25}$$

Figure 2.4: Asteroid Itokawa imaged from 8 kilometers by JAXA's Hayabusa spacecraft in 2005

Once the gradient of the potential has been computed, the acceleration can be obtained as in Eq. (2.26)

$$\mathbf{a}_{ell} = -\frac{3}{2} GM\mathbf{r} \int_{\lambda}^{\infty} \frac{du}{(\xi + u)\Delta(u)} \tag{2.26}$$

Where ξ is α^2 when computing the first component, β^2 when computing the second component and γ^2 when computing the third component.
By performing the second derivatives, the Jacobian of the acceleration can be computed as shown in Eq. (2.27)

$$\nabla \mathbf{a}_{ell} = -2G\rho\pi\alpha\beta\gamma \begin{bmatrix} U_{xx} & U_{xy} & U_{xz} \\ U_{xy} & U_{yy} & U_{yz} \\ U_{xz} & U_{yz} & U_{zz} \end{bmatrix} \tag{2.27}$$

where:

$$U_{xx} = \int_{\lambda}^{\infty} \frac{du}{(\alpha^2 + u)\Delta(u)} - \frac{2x^2}{(\alpha^2 + \lambda)^2 \Delta(\lambda)\psi}$$

$$U_{yy} = \int_{\lambda}^{\infty} \frac{du}{(\beta^2 + u)\Delta(u)} - \frac{2y^2}{(\beta^2 + \lambda)^2 \Delta(\lambda)\psi}$$

$$U_{zz} = \int_{\lambda}^{\infty} \frac{du}{(\gamma^2 + u)\Delta(u)} - \frac{2z^2}{(\gamma^2 + \lambda)^2 \Delta(\lambda)\psi}$$

$$U_{xy} = -\frac{2xy}{(\alpha^2 + \lambda)(\beta^2 + \lambda)\Delta(\lambda)\psi}$$

$$U_{xz} = -\frac{2xz}{(\alpha^2 + \lambda)(\gamma^2 + \lambda)\Delta(\lambda)\psi}$$

$$U_{yz} = -\frac{2yz}{(\beta^2 + \lambda)(\gamma^2 + \lambda)\Delta(\lambda)\psi}$$

with:

$$\psi = \frac{x^2}{(\alpha^2 + \lambda)^2} + \frac{y^2}{(\beta^2 + \lambda)^2} + \frac{z^2}{(\gamma^2 + \lambda)^2}$$

Mascon Model

Another possible approach is to discretize the asteroid by considering N concentrated masses. This strategy is particularly convenient from the computational point of view. The resulting gravity field will be the sum of the multiple central fields:

$$\ddot{\mathbf{r}} = G\sum_{i=1}^{N}\frac{m_i}{|r_i|^3}\mathbf{r}_i \tag{2.28}$$

This method is particularly indicated for inhomogeneous asteroids that cannot be modelled with constant density shapes. However, this kind of application is effective only if the distribution of the point masses is similar to the real mass distribution. Simulation of the asteroid aggregation process can help from this point of view.

2.3 State transition matrix

As clearly shown in Chapter 4, the trajectory design in the non-Keplerian environment close to the asteroid will require the use of a Newton's method to solve for the initial state, given some constraints on the final state. To do that, the State Transition Matrix (STM) is needed. The STM is the derivative of the flow generated by the N-body vector field with respect to initial conditions as shown in Eq. (2.29)

$$\mathbf{\Phi}(t, t_0) = \frac{\partial \mathbf{X}}{\partial \mathbf{X}_0} \tag{2.29}$$

where $\mathbf{X}$ is the n-dimensional state vector of the system of nonlinear differential equations in Eq. (2.30) and initial conditions $\mathbf{X}_0$.

$$\dot{\mathbf{X}} = \mathbf{f}(\mathbf{X}) \tag{2.30}$$

Rigorously, the evaluation of the STM is done by solving the variational equations as additional differential equations to the previous system that becomes:

$$\begin{cases} \dot{\mathbf{X}} = \mathbf{f}(\mathbf{X}) \\ \dot{\mathbf{\Phi}}(t, t_0) = \mathbf{J}(t)\mathbf{\Phi}(t, t_0) \end{cases} \tag{2.31}$$

where $\mathbf{J}$ is the Jacobian of the vectorial field as shown in Eq. (2.32)

$$\mathbf{J} = \frac{\partial \mathbf{f}}{\partial \mathbf{X}} \tag{2.32}$$

2.4 Non gravitational perturbations: Solar Radiation Pressure

Due to their relatively small mass, other non-gravitational perturbations can be considered not negligible when dealing with spacecraft dynamics around asteroids. Among these, the effect of the Solar Radiation Pressure (SRP) is the most relevant for our case. In this work, SRP has been modelled with a simple cannonball model[34] as shown in Eq. (2.33):

$$\mathbf{a}_s = \frac{A}{m}(1+C_r)\frac{P_0}{c}\left(\frac{R_{SE}}{R_{SS}}\right)^2\frac{\mathbf{R}_{SS}}{|\mathbf{R}_{SS}|} \tag{2.33}$$

where $\frac{A}{m}$ is the area-to-mass ratio of the spacecraft facing the Sun, C_r is the reflectivity, P_0 is the solar power measured at the Earth (1346 W/m^2), c is the speed of light, R_{SE} is the Sun-Earth distance (1 AU) and $\mathbf{R}_{SS}$ is the Sun-spacecraft position vector.

Chapter 3

Dynamical system

The motion close to small bodies usually deviates significantly from the familiar Keplerian orbits due to their small and irregular gravity field and not negligible perturbations as Solar Radiation Pressure. Additionally, in case of a binary target, the resultant three body problem would significantly complicate the trajectory design around the asteroid. To successfully orbit in such a challenging environment, an understanding of the orbital dynamics is mandatory and a reliable model of the entire ambient is the key point for a successful mission design.
In this chapter, the description of the dynamical system introduced to simulate the motion around Didymos is present. In Section 3.1 there is information on the case study under investigation. Section 3.2 is about the reference frames used during the simulations, while in Section 3.3 there is a description of the dynamical model used and its validation with the ESA data about Hera. Section 3.4 shows the results obtained by the modelling of the gravity field with the use of a point-like model, spherical harmonics and an ellipsoid shape model. After a comparison between the results, the minimum distance at which the point-like model is reliable is highlighted.

3.1 Case study

The mission

In this section, the case study under investigation is introduced. As mentioned in Chapter 1, this thesis concerns the European contribution to the AIDA mission. As a NASA-ESA joint mission, AIDA is the first planetary defense mission aimed to investigate the kinetic impactor technique for deflecting a small body. After the impact on the asteroid by DART, the American spacecraft, ESA will control his mothership Hera near the body, with the aim of investigating the effects of this impact. In proximity of Didymos, Hera will

deploy two CubeSats with the aim of performing even closer observations of the body by acting as a proxy for these two. Also being the first in-depth inspection of a binary asteroid, the mission represents a milestone in the European space exploration.
In particular, this work deals with possible close trajectories for Hera's second CubeSat, Milani.

The asteroid

65803 Didymos is a binary Near Earth Asteroid of both Apollo and Armor group since it crosses the orbit of both Earth and Mars. Its orbital and physical properties are depicted in Table 3.1. As shown in Table 3.1, the asteroid's perihelion is just below the aphelion radius of Earth orbit. Therefore, Didymos poses no particular threat to Earth, making him a good subject for the first planetary defense experiment.

Orbital Parameters			
$\mathbf{a_H}$	$\mathbf{p_H}$	**a**	**e**
2.2760 AU	1.0133 AU	1.66446 AU	0.3839
i	**T**	**n**	$\mathbf{a_{orb}}$
3.4083°	770 days	0.4673°/day	1.18 km
Physical Parameters			
$\mathbf{R_{g1}}$		$\mathbf{R_{g2}}$	
(0.832, 0.837, 0.786) km		(0.082, 0.063076, 0.0525641) km	
$\mathbf{M_1}$	$\mathbf{M_2}$	$\mathbf{M_2/M_1}$	ρ_{bulk}
$5.226\text{x}10^{11}$ kg	$4.860\text{x}10^{9}$ kg	0.0093	2146 kg/m^3

Table 3.1: Didymos' orbital and physical properties. A complete description of the nomenclature used is present in the list of symbols at the end of the thesis.

Additional peculiarities not present in the table can be said about Didymos. The asteroid is a synchronous binary system, which means that Didymoon orbits around Didymain with a period equal to the average rotational period of the primary. This, coupled with the assumption of zero relative inclination between the orbital planes of the asteroids, makes the natural satellite facing the same Didymain area as a geostationary satellite does with the Earth. Furthermore, the same plane also coincides with the equatorial plane of the primary asteroid.

3.2 Reference frames

In this section, the reference frames used during the simulations are described. Generally, two kinds of reference frame were used:

- **Inertial reference frames**: all the integrations were done using an inertial reference frame. During the first propagations in this chapter the J2000 reference frame was used. In this work, this frame is centered in the binary system barycenter, has the x-axis pointing to the Vernal Equinox at epoch J2000, the z-axis perpendicular to the mean Earth's equatorial plane at epoch J2000 and the y-axis that completes the right-hand frame. In Chapter 5 the inertial frame used was the ECLIPJ2000 which is similar to the J2000 with the difference of having the z-axis perpendicular to the mean ecliptic plane at epoch J2000.

- **Non-Inertial reference frames**: These frames were used to assess the gravity potential of the asteroids or to impose constraints and show the results in Chapter 5. Complex gravity fields were computed using body-fixed reference frames which are centered in the body's barycenter with the axis parallel to the principal axis of the body. To impose constraints on close trajectories and show them, a Didymos Equatorial Sun South reference frame was conceived. This frame is centered in the system barycenter, has its z-axis parallel to the south pole of the asteroid, its x-axis as the projection of the Sun direction on the equatorial plane and the y-axis completing the right-hand frame. The frame is shown in Fig. 3.1.

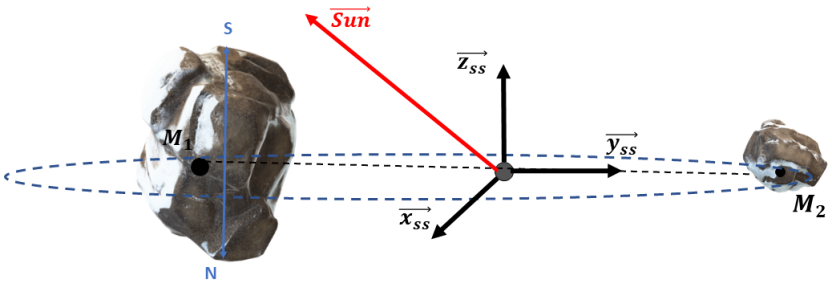

Figure 3.1: Didymos Equatorial Sun South reference frame.

3.3 Dynamical setting

The aim of this section is to reproduce the dynamical environment around Didymos in a high fidelity model in order to reliably propagate proximity trajectories in Chapter 5. The forces and perturbations acting on a mass-less body orbiting around Didymos are studied and their orders of magnitude are compared with each other.
All simulations around Didymos were conducted in an inertial reference frame centered in the system barycenter. Consequently, the system of differential equations solved is similar to the one seen for a Restricted Three Body problem (Eq. (2.4)) with a richer right-hand side as in Eq. (3.1)

$$\ddot{\mathbf{R}} = \frac{\partial U_1}{\partial \mathbf{R}_1} + \frac{\partial U_2}{\partial \mathbf{R}_2} + \mathbf{a}_p + \mathbf{a}_0 \tag{3.1}$$

Together with the gravitational contributions of the two asteroids, two additional accelerations were considered. $\mathbf{a}_p$ collects all the perturbations introduced by additional gravity sources (Eq. (3.2)) and SRP (Eq. (2.33)), while $\mathbf{a}_0$ is the relative acceleration that the binary system barycenter feels since it moves around the Sun (Eq. (3.3)).

$$\mathbf{a}_p = \sum_i^n -GM_i \left(\frac{\mathbf{r} - \mathbf{r}_i}{|\mathbf{r} - \mathbf{r}_i|^3} \right) + \mathbf{a}_s \tag{3.2}$$

$$\mathbf{a}_0 = \sum_i^n -GM_i \frac{\mathbf{r}_i}{|\mathbf{r}_i|^3} \tag{3.3}$$

here, G is the universal gravity constant, $\mathrm{M_i}$ is the mass of the i-th of the n bodies considered, $\mathbf{r}$ is the position of the mass-less particle, $\mathbf{r}_i$ is the position of the i-th body considered and $\mathbf{a}_s$ is the SRP shown in Eq. (2.33).
All the information used in the simulations on the celestial bodies involved, including their states at every time instants and their physical properties, were taken from the kernels present in the ESA database*. The spacecraft's parameters needed for the evaluation of the SRP were provided courtesy of Dr. Fabio Ferrari and are depicted in Table 3.2

*https://www.cosmos.esa.int/web/spice/spice-for-hera

m [kg]	A [m^2]	C_r
512	10	0.5

Table 3.2: Hera physical parameters needed for the correct evaluation of the SRP.

The integration has always been conducted with the use of a Adams-Bashforth-Moulton method of orders 1 to 13. However, the highest possible order used is 12, since 13 is used for error estimation with the solution given at a order 13 only due to local extrapolation. The algorithm used is the built-in `ode113.m` in Matlab.

Setting validation

To validate the dynamical setting used, ESA kernels about the motion of Hera around Didymos were used. The considered epoch starts on the 28^{th} of Jan 2027 at 08:17:00 et and ends on the 31^{st} of Jan 2027 at 08:15:00 et. The results shown in Fig. 3.2, Fig. 3.3, Table 3.4 and Fig. 3.4 were obtained using spherical harmonics. There is no need of showing the performances of the other models due to the similarity of the results. Table 3.3 shows the difference in terms of maximum relative error, while the complete comparison between the different gravity models considered is present in the second part of this section.

Point-like	Spherical harmonics	Ellipsoid
7.20893×10^{-3}	7.20821×10^{-3}	7.20850×10^{-3}

Table 3.3: Maximum relative error using different models obtained at a distance of 45 km during the considered trajectory around Didymos in the integration time [28 Jan 2027 - 31 Jan 2027]. The error considered is the norm of the difference between the propagated position and ESA's ephemerides divided by the norm of the ephemerides.

Didymain	Didymoon	Earth	Sun	Jupiter	SRP
5.7×10^{-11}	5.3×10^{-13}	1.4×10^{-11}	8.9×10^{-06}	3.0×10^{-10}	1.9×10^{-10}

Table 3.4: Mean value of the involved accelerations acting on Hera expressed in km/s^2 evaluated in between 30 and 48 km.(Here only the absolute accelerations are shown without the relative acceleration due to the not perfectly inertial reference frame used).

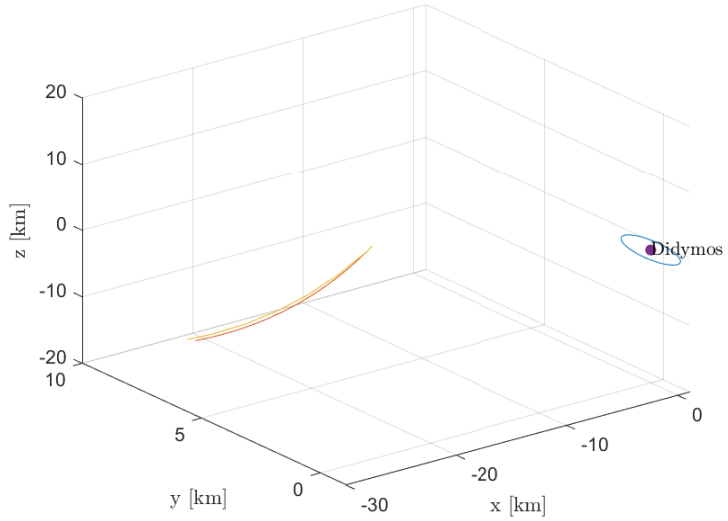

Figure 3.2: Hera trajectory around Didymos in the integration time [28 Jan 2027 - 31 Jan 2027] in the J2000 reference frame. The red line is the real trajectory, the orange line is the propagated orbit and the blue orbit is Didymoon around Didymos.

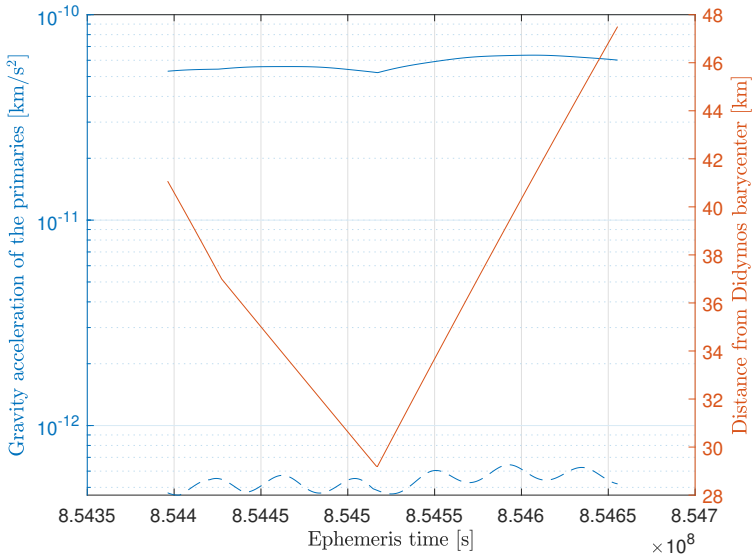

Figure 3.3: Order of magnitude of the acceleration on Hera due to Didymain (continuous blue line) and Didymoon (dashed blue line) compared with the distance from the binary system barycenter (red line).

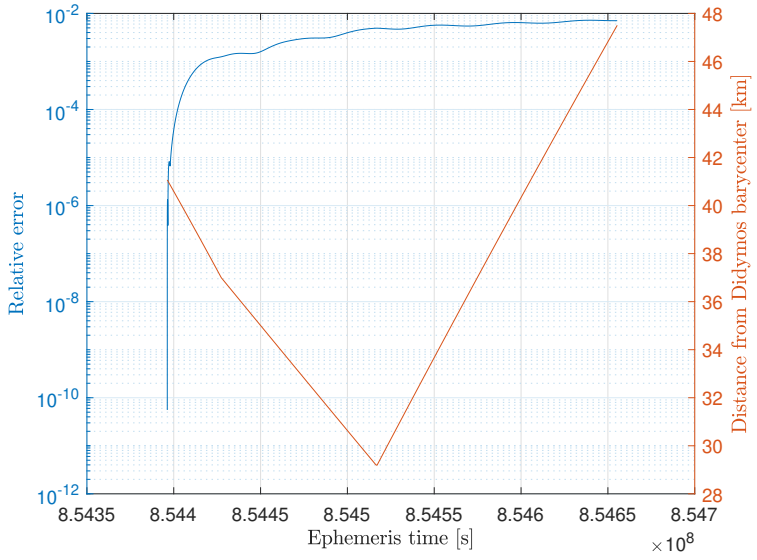

Figure 3.4: Relative error (blue line) compared with the distance from the binary system barycenter (red line). The error considered is the norm of the difference between the propagated position and ESA's ephemerides divided by the norm of the ephemerides.

Fig. 3.3 shows how the gravity field of the primary is practically unaffected by its motion around the system barycenter, differently from the one belonging to the secondary. This is due to the fact that the barycenter of the primary is very close to the one of the binary system with a relative distance of the order of tens meters. Furthermore, it seems that the higher the distance the higher the gravitational attraction. However, this unexpected non-physical effect can be attributed to some numerical issue as the maximum increment is in the order of 10 nm/s^2 after a variation of 10km from the system barycenter.
Table 3.3 shows no appreciable difference between the gravity models considered. This is probably due to the fact that Didymain's shape is close to a sphere and at this distance the difference between the models is not remarkable.
It should be noted that the trajectory shown in Fig. 3.2 is part of a longer orbit around Didymos and shows a ballistic arc between two maneuvers. The full trajectory with all maneuvers is depicted in Fig. 3.5. The performances of the full trajectory are not shown since they are a cyclic repetition of the one already shown.

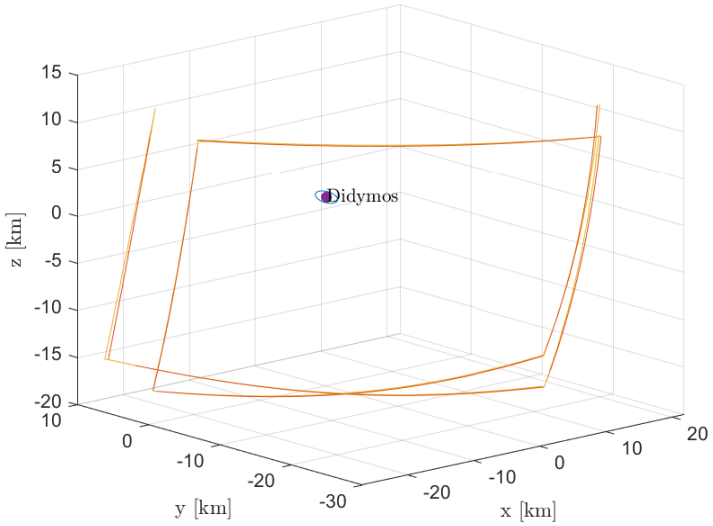

Figure 3.5: Full orbit around Didymos in the integration time [28 Jan 2027 - 25 Feb 2027] in the J2000 reference frame. The red line is the real trajectory, the orange line is the propagated orbit and the blue orbit is Didymoon around Didymos.

3.4 Different gravity models

In this section, the asteroids' gravity field is modelled following different strategies. The aim is to build a reliable characterization of the vector field in close proximity of the asteroid where the point-like model is no longer trustfully. Together with the point-like model, the strategies considered as alternatives are the use of spherical harmonics and the ellipsoidal-shape model.
Spherical harmonics coefficients were taken from [35] and are depicted in Table 3.5. For the simulations, Didymain was modelled up to the 4^{th} order while Didymoon up to the 2^{nd}.

Order l	**Degree m**	$\mathbf{C_{l,m}}$	$\mathbf{S_{l,m}}$
0	0	1.0	-
1	0	0	-
1	1	0	0
2	0	-6.3422×10^{-2}	-
2	1	0	0
2	2	4.0949×10^{-3}	0
3	0	-1.5154×10^{-3}	-
3	1	2.8455×10^{-4}	1.1578×10^{-4}
3	2	2.89891×10^{-5}	-1.89599×10^{-5}
3	3	3.995×10^{-4}	-1.293×10^{-4}
4	0	4.066049×10^{-2}	-
4	1	-2.65537×10^{-5}	3.352119×10^{-5}
4	2	-9.588539×10^{-5}	-1.28121×10^{-6}
4	3	-8.305724×10^{-6}	-4.819896×10^{-6}
4	4	3.544874×10^{-5}	-7.124178×10^{-6}

(a)

Order l	**Degree m**	$\mathbf{C_{l,m}}$	$\mathbf{S_{l,m}}$
0	0	1.0	-
1	0	0	-
1	1	0	0
2	0	-9.8273×10^{-2}	-
2	1	0	0
2	2	2.6374×10^{-2}	0

(b)

Table 3.5: Unnormalized exterior spherical harmonic coefficients of (a) Didymain and (b) Didymoon.

To find the minimum altitude at which the point-like model is still reliable, a vector of distances between 0.8 km and 4 km from the binary system barycenter has been considered. For each distance the gravity field of the asteroids was evaluated in all three gravity models previously discussed at a given time instant (28 Jan 2027 08:17:00 et). Then, by measuring the relative error (norm of the difference between the propagated position and ESA's ephemerides divided by the norm of the ephemerides) between the point-like model, the spherical harmonics model and the ellipsoid shape model the minimum distance has been found. The maximum admissible relative error was of 1%. Assuming the point-like model the worst approximation for the asteroid, from Fig. 3.6 spherical harmonics appears to be the most accurate strategy. Compared to it, the point-like model gives a minimum altitude of 2.74km at which the error is 1%. Differently, the ellipsoid model deviates from the point-like model at lower altitudes with a minimum distance of 1.46km.

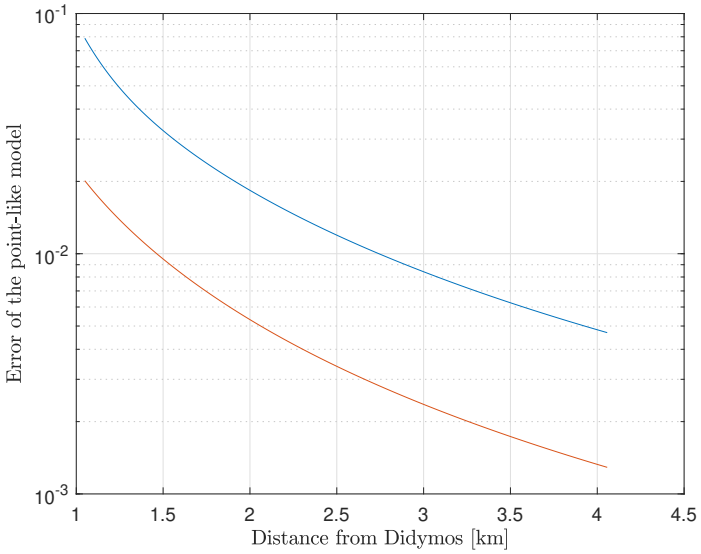

Figure 3.6: Relative error of the point-like model with respect to spherical harmonics (blue) and ellipsoid-shape model (red). The error is computed with the norm of the difference between the positions considered divided by the norm of the complex gravity model considered.

Chapter 4

Numerical Methods

One of the biggest challenge about non-Keplerian dynamics is finding solutions that suit the mission requirements. The chaotic environment of a three body problem, the strong non-linearity and the absence of analytical solutions make the design of generic orbital solutions problematic. Numerical methods are the most powerful tool that can be used to deal with these problems. With them, few particular solutions such as periodic orbits have been extensively studied for a three-body system. However, the problem is far from being considered well treated. In this section, the numerical methods used to compute trajectories in a non-Keplerian system are present.

4.1 Generic software architecture for non-Keplerian trajectories

In this chapter, a generic software architecture used to propagate orbits in a non-Keplerian environment is present. The aim is to show a general purpose algorithm that can be used for any desired orbit. The basic architecture is composed by two main blocks, as shown in Fig. 4.1: a good initial solution, fundamental due to the strong non-linearity of the dynamical environment and a correction method to converge to the desired trajectory. The correction strategy is based on the imposition of a constraint on the solution of the propagation in order to obtain a desired final state.

Initial Guess

The initial guess will be the starting point used by the algorithm to approximate the trajectory for the first time. As entrance value, its proximity to the desired initial condition is important to aim to convergence. The initial guess will be made by the initial state of the spacecraft. The considered problem is focused on finding the trajectory connecting two desired points. Consequently,

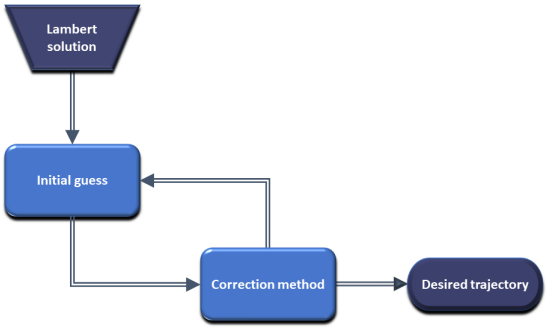

Figure 4.1: Graphical representation of the algorithm used to find the trajectories.

the initial position will already be the corrected one, while as a guess for the initial velocity, the solution of a Lambert problem involving the primary asteroid as gravity source can be used. It is clear that the dynamic is far from being an unperturbed two body problem as described in the Lambert problem. However, Lambert's solution seems to be the best starting point for the algorithm. To increase efficiency, particular attention can be paid to the prograde or retrograde expected nature of the transfer.

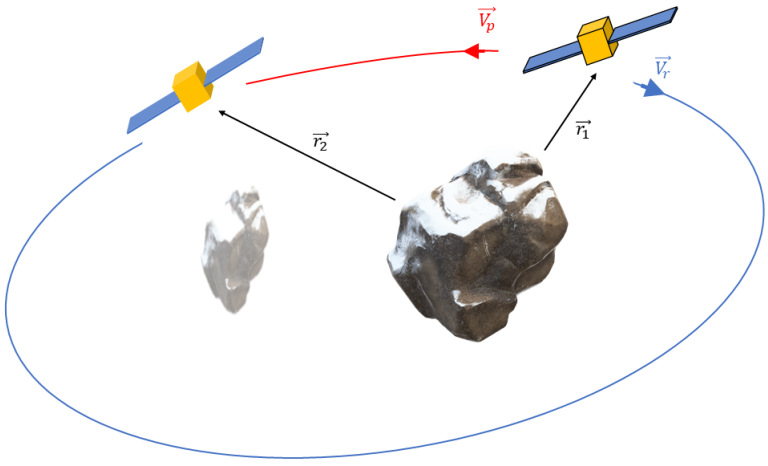

Figure 4.2: Sketch of the Lambert problem solution were only Didymain is considered as source of gravity.

Clearly, the initial position is given as well as the final position as desired maneuver points.

Correction method: Differential Correction

With a good initial guess, an approximation of the desired trajectory is obtained and must be corrected in order to fulfill the desired constraints onto the final state of the spacecraft. Applying a correction method is equivalent to solving a boundary value problem in which some of the initial conditions are missing and must be obtained using some information on the other boundary. The most common correction method is the use of differential corrections. The application is straightforward and requires two steps: the definition of the constraints to be satisfied on the final state and the identification of the free variables that the algorithm can change.
Correction methods have been widely used enforcing periodicity constraints searching for periodic orbits[36]. However free variables and constraints depend only on the desired orbit. In this work, a condition on the final position has been enforced, considering as free variables the components of the initial velocity. The simplest implementation of differential corrections is an iterative Newton's method as shown in Eq. (4.1)

$$\mathbf{X}_g^{k+1} = \mathbf{X}_g^k - \nabla \mathbf{G}(\mathbf{X}_g^k) \tag{4.1}$$

This algorithm moves from the previous guess $\mathbf{X}_g^k$ in the direction of the negative gradient of the objective function $\mathbf{G}(\mathbf{X}_g^k)$.
For our purpose, the vector $\mathbf{X}_g^k$ represents the initial velocity at the the k-th step, while the gradient of the objective function is the product between the inverse of the Jacobian and the error between the propagated final position and the desired one (Eq. (4.2)).

$$\nabla \mathbf{G}(\mathbf{X}_g^k) = \mathbf{J}(\mathbf{X}^k)^{-1}\mathbf{F}(\mathbf{X}^k) \qquad \mathbf{F}(\mathbf{X}^k) = \mathbf{X}_{end}^k - \mathbf{X}_{end}^d \tag{4.2}$$

The Jacobian is found by computing the derivatives of the constraints with respect to free variables. As such, the Jacobian is built using the components of the STM defined in Section 2.3 as the derivative of the state with respect to a variation of the initial condition.
In the case of an under-constrained problem, the solution can be found using the Moore-Penrose (pseudo) inverse of the Jacobian as in Eq. (4.3)

$$\mathbf{X}_g^{k+1} = \mathbf{X}_g^k - \mathbf{J}(\mathbf{X}^k)^\top \left[\mathbf{J}(\mathbf{X}^k)\mathbf{J}(\mathbf{X}^k)^\top\right]^{-1}\mathbf{F}(\mathbf{X}^k) \tag{4.3}$$

Newton's algorithm is only a particular method of the more general gradient descent algorithm, for which the stepsize of the correction factor is not unitary. More powerful than Newton's algorithm, this generalization can be useful when convergence problems arise. As a drawback, this strategy can slow down convergence and for that reason is only suggested when necessary.

The algorithm and the computation of the stepsize are shown in Eq. (4.4) and Eq. (4.5)

$$\mathbf{X}_g^{k+1} = \mathbf{X}_g^k - \gamma_k \nabla \mathbf{G}(\mathbf{X}_g^k) \tag{4.4}$$

$$\gamma_k = \frac{|(\mathbf{X}_g^k - \mathbf{X}_g^{k-1})^\top [\nabla \mathbf{G}(\mathbf{X}_g^k) - \nabla \mathbf{G}(\mathbf{X}_g^{k-1})]|}{||\nabla \mathbf{G}(\mathbf{X}_g^k) - \nabla \mathbf{G}(\mathbf{X}_g^{k-1})||^2} \tag{4.5}$$

γ should be small enough to guarantee that the next value of the error function will be lower than the precedent. There are several ways to find the right γ (e.g. via line search or the Barzilai–Borwein method[37] seen in Eq. (4.5)).
Once the correction algorithm has been chosen, its implementation can be done considering either a single-shooting strategy or a multiple-shooting strategy. Single shooting algorithms foresee a single integration over the whole arc, while multiple-shooting strategies discretize the trajectory into a series of patch points. The sub-arcs are integrated independently and the problem is enriched by enforcing continuity at the end and at the begging of each consecutive arc in order to form a single trajectory. Although the constraints grow significantly as the number of patch points increases, multiple-shooting algorithms seem to be more powerful than single-shooting ones, in general.

4.2 State Transition Matrix

As seen in Section 4.1, the evaluation of the State Transition Matrix is an important step for computing trajectories in a non-Keplerian environment. Section 2.3 shows how the STM can be obtained analytically without any approximations. However, solving variational equations can be both computational expensive and troublesome, especially when using complex gravity models. A valid alternative is to compute the Jacobian of the vector field with the use of finite difference methods.
The idea is to capture the variation of the final conditions given a perturbation dx of the initial condition with a simple Euler formula as shown in Eq. (4.6)

$$\mathbf{J} = \frac{\mathbf{X}_f(\mathbf{X}_0 + dx) - \mathbf{X}_f(\mathbf{X}_0)}{dx} \tag{4.6}$$

To save time, only the derivative with respect to the free variables considered in Section 4.1 should be computed in order to directly obtain the Jacobian without evaluating the entire State Transition Matrix.

Chapter 5

Results

The prime ambition of this work is to explore the dynamical environment close to a binary asteroid and propose proximity solutions for future observation strategies. All proposed trajectories start on 19$^{\text{th}}$ May 2027 at 00:00:02 et and have been obtained with the same dynamical setting seen in Chapter 3 and the same algorithm described in Chapter 4.
Differently from the results shown in Section 3.3, the spacecraft is now a CubeSat with the physical parameters depicted in Table 5.1.
The case study is related to Didymos, target of the AIDA mission. As a mission requirement, the CubeSat shall be always in sunlight to successfully adopt optical navigation close to the asteroid. As a consequence, all the maneuver points were placed in the illuminated subspace around Didymos. To easily impose such requirement, a new reference frame has been conceived in which the maneuver points are defined and the results are shown. The new reference frame, centered in the system barycenter, has the xy plane coincident with the equator of the asteroid, the z-axis pointing to its South pole and the x-axis as the projection of the direction pointing the Sun onto the equator. This new reference frame is depicted in Fig. 3.1.
Two orbit shapes have been investigated and proposed for the proximity operations around Didymos. For both, a grid search strategy has been adopted to explore their capabilities and stability around the asteroid. Section 5.1 shows a loop cycle solution close to the equator, able to produce flexible results in terms of distance from the binary system. Promising is the possibility of orbiting in quasi-circular trajectories explored with this shape. Differently, Section 5.2 offers the possibility to orbit also far away from the equator in order to observe polar zones. The relative solutions offered are numerous, especially in terms of maneuver points position and duration of the ballistic arcs.

m [kg]	A [m^2]	C_r
12	0.516	0.193

Table 5.1: CubeSat physical parameters needed for the correct evaluation of the SRP.

5.1 Loop cycle trajectories

Loop cycles are orbits designed to approach as close as possible the asteroid, while respecting the constraint on solar illumination. They consist of single arcs that can be endlessly repeated or alternated each other. While their design is easy as it is based on maximizing the distance between the points, their performance is outstanding as it is shown in Section 5.1. Furthermore, their scientific relevance is excellent since with them it is possible to observe the same region while preserving the same features in terms of distance and phase angles for a theoretical infinite amount of time. The main drawback is that regions of high declination are almost never covered during these orbits.
In this section, the design of the maneuver points for a loop cycle shape orbit close to Didymos is shown. The trajectory degrees of freedom are highlighted and a grid search aimed to find the effects of their variation onto the orbit performance is described. Finally, some possible solutions are shown and commented.

Desired maneuver points design

Being a loop cycle, this shape allows for an unconstrained large number of maneuver points. Therefore, each one can be retrieved with the same rationale. After the imposition of the constraints related to the subspace always illuminated by the Sun, each couple of points of these trajectories are found maximizing their distance. This helps the spacecraft get closer to the asteroid by positioning the perigee of its trajectory as near as possible to the middle point of the line connecting the two points. As a consequence, an additional constraint is enforced onto the radial position of this middle point. All the maneuvers points are also taken at the same distance from the system barycenter.
Following this strategy, together with close hyperbolic arcs, relevant quasi-circular trajectories have been obtained.

Loop grid search

A grid search algorithm has been used to explore the performances of these trajectories after the variation of its degrees of freedom. The goal is to check

the trajectory stability and investigate which configuration can ensure quasi-circular orbits.
The loop cycle has 3 degrees of freedom: the distance at which the maneuver points are located, the distance at which the middle point between them is positioned and the duration of the parabolic arc. The values considered for them are all depicted in Table 5.2.

$\mathbf{R}$	1.5,2,3,4,5,6,7,8,9,10
$\mathbf{X_m}$	0.5,1,2,3,4,5,6
$\mathbf{\Delta t_1}$	1,2,3

Table 5.2: Candidate distances from the system barycenter, position of the middle point and duration of the parabolic arc considered. Distances are expressed in km while duration in days.

For each value of $\mathbf{R}$, the maneuver points are found by maximizing the distance between them and forcing the middle point to be in each position considered. Then the trajectory between the two points is computed for all the time spans considered. If the trajectory is stable, the solution is marked with a green dot. If the distance of the perigee from the system barycenter is less than 1km different with respect to the one of the maneuver points, the solution is marked with a gold dot to highlight the possible quasi-circular orbit. In case the solution is unstable it is marked with black dot. The results are shown in Fig. 5.1 and Table 5.3.

$\Delta t \backslash X_m$	0.5	1	2	3	4	5	6
1	3-4	3-4	4	4-5	5-6	6	6-7
2	5	5-6	5-6	6-7	7	7-8	8-9
3	6-7	7	7-8	8	8-9	9-10	9-10

Table 5.3: Range of distances, values of duration and middle points distance at which a quasi-circular trajectory is obtained. Distances are expressed in km while durations in days.

From Fig. 5.1 it is possible to capture the behaviour of the perigee of close trajectories around Didymos as function of the position of the two boundary points and the duration of the ballistic arc. As expected, the shorter the time imposed to perform the arc, the closer the perigee, since the spacecraft is forced to reach the end of the trajectory faster. Graphically, it is as if the spacecraft were forced to perform a trajectory as close as possible to the shortest track, the straight line connecting the two boundary points.

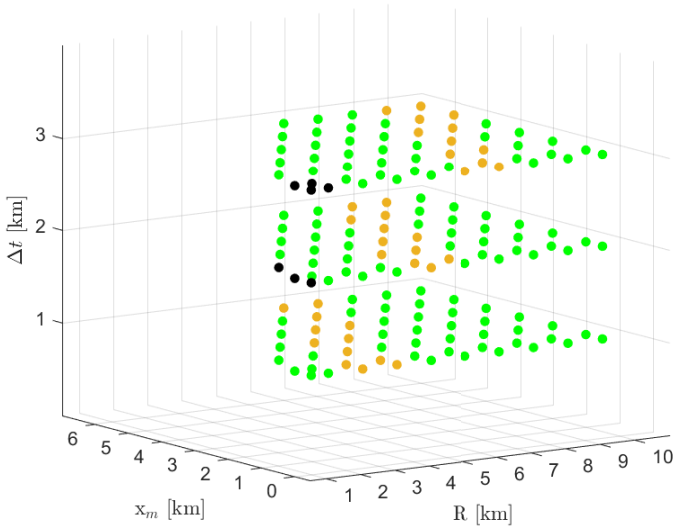

Figure 5.1: Results from the stability analysis on loop cycle trajectories. The black dots are unstable solutions, the green dots are stable solutions and the gold dots are quasi-circular arcs.

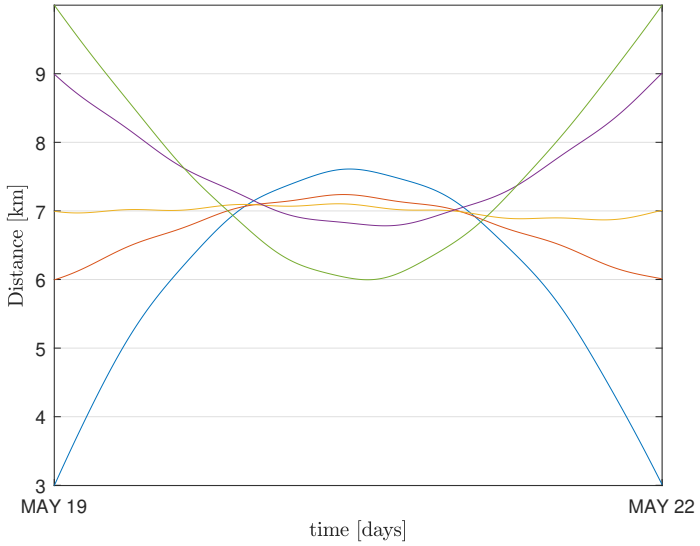

Figure 5.2: Distance from Didymain of a single arc of 3 days between points at: 3km (blue), 6km (red), 7km (orange), 9km (purple), 10km (green). For all the points the middle point of the line connecting them is at 500m from the system barycenter.

Therefore, the closer the middle point of the straight line connecting the dots is to the lowest perigee possible at that time, the more circular the trajectory. An example of this behaviour is shown in Fig. 5.2.
From the figure, three operative regions can be distinguished:

- For maneuver points placed at an altitude higher than 7km, trajectories with perigee at a minimum of about 6km are possible. In this region, orbits with maneuvers far from the asteroids are present
- For maneuver points placed at an altitude in between 6km and 7km, quasi-circular trajectories are possible. This is the boundary between the first and the third region
- For maneuver points placed at an altitude lower than 6km, trajectories with maneuvers as closest points are possible. In this region, the only possibility to get closer to the asteroid is to place the maneuver points at low altitude. As a result, the apogee of the trajectory will always be about 7km from the asteroid.

By looking for the gold dots in Fig. 5.1 and looking at Table 5.3, other regions can be identified for 2-day and 1-day maneuver frequencies. The best performance is possible with the midpoint placed as close as possible to the asteroid. However, different regions occurs with middle points placed farther from the asteroid. In Fig. 5.3 it is possible to see the behaviour of some solutions as the time between the arc or the position of the middle point changes.

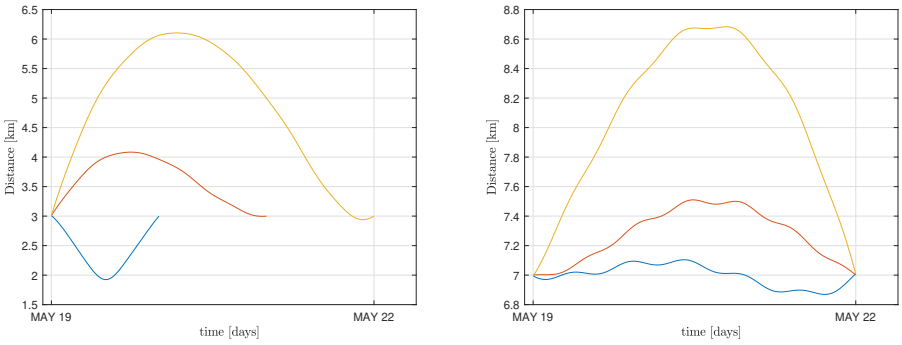

(a) **(b)**

Figure 5.3: a) Distance from Didymain of trajectories with points at 3km with the middle point at 2km in: 1 day (blue), 2 days (red), 3 days (orange). b) Distance from Didymain of trajectories with points at 7km in 3 days with the middle point at: 0.5 km (blue), 2m (red), 4km (orange). The high frequency oscillations are due to the motion of the primary around the system barycenter.

Possible loop trajectory solutions

Here, some possible solutions with a loop cycle shape are shown.
In Fig. 5.4 trajectories with maneuver points at lower altitudes with respect to the other points are present. Three different solutions have been proposed with manevuers each 3 days, 2 days and 1 day.
In Fig. 5.5 quasi-circular trajectories are present. As before, three different solutions have been proposed with manevuers each 3 days, 2 days and 1 day. These figures have the role of showing the possibilities of flying at quasi-constant altitudes. However, for safety reason it is possible to explore distances slightly different from the one offering quasi-circular trajectories.
In Fig. 5.6 trajectories with maneuver points at higher altitudes with respect to the ohter points are present. Also for them, three different solutions have been proposed with manevuers each 3 days, 2 days and 1 day. These shapes may be preferred to the one in Fig. 5.4 since performing scientific measurements far away from the maneuvers is always recommended. In Table 5.4 the costs for all the maneuvers present in the solutions shown are depicted.
Additionally, peculiar solutions can be obtained using different combinations of the arcs shown in Fig. 5.1. These trajectories can be useful in case a more relaxed maneuver frequency is needed as in Fig. 5.7 or in case the maneuver points must be placed far from the asteroid as in Fig. 5.8. The costs of these alternative solutions are depicted in Table 5.5.

ΔV_1	ΔV_2	ΔV_3
16.80	16.83	16.96

(a) Cost of Fig. 5.4a

ΔV_1	ΔV_2	ΔV_3
23.98	24.08	23.61

(b) Cost of Fig. 5.4c

ΔV_1	ΔV_2	ΔV_3
35.62	35.17	42.77

(c) Cost of Fig. 5.4e

ΔV_1	ΔV_2	ΔV_3
15.48	15.67	15.92

(d) Cost of Fig. 5.5a

ΔV_1	ΔV_2	ΔV_3
18.13	17.86	18.11

(e) Cost of Fig. 5.5c

ΔV_1	ΔV_2	ΔV_3
20.53	20.55	20.77

(f) Cost of Fig. 5.5e

ΔV_1	ΔV_2	ΔV_3
16.02	15.96	15.95

(g) Cost of Fig. 5.6a

ΔV_1	ΔV_2	ΔV_3
17.73	17.49	17.72

(h) Cost of Fig. 5.6c

ΔV_1	ΔV_2	ΔV_3
22.70	22.55	22.73

(i) Cost of Fig. 5.6e

Table 5.4: Cost of the loop maneuvers in cm/s.

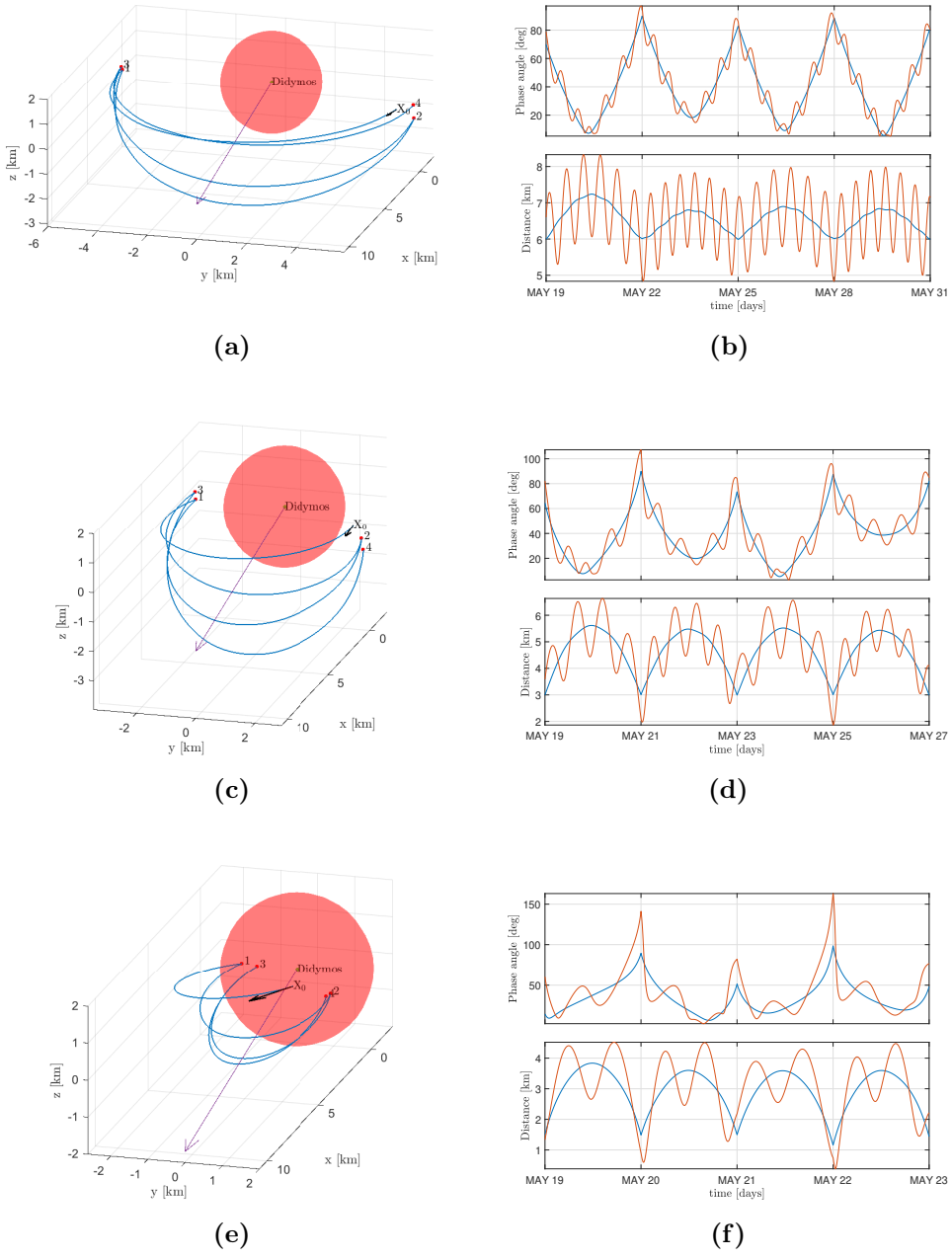

Figure 5.4: Loop trajectories with perigee at higher altitudes. a-b) Points at 6km, arc of 3 days. c-d) Points at 3km, arc of 2 days. e-f) Points at 1.5km, arc of 1 day. In purple the direction pointing the Sun. Next to the trajectories: the phase angle (Sun-asteroid-CubeSat) (up). The distance (down). In blue the data with respect to Didymain, in red the data with respect to Didymoon.

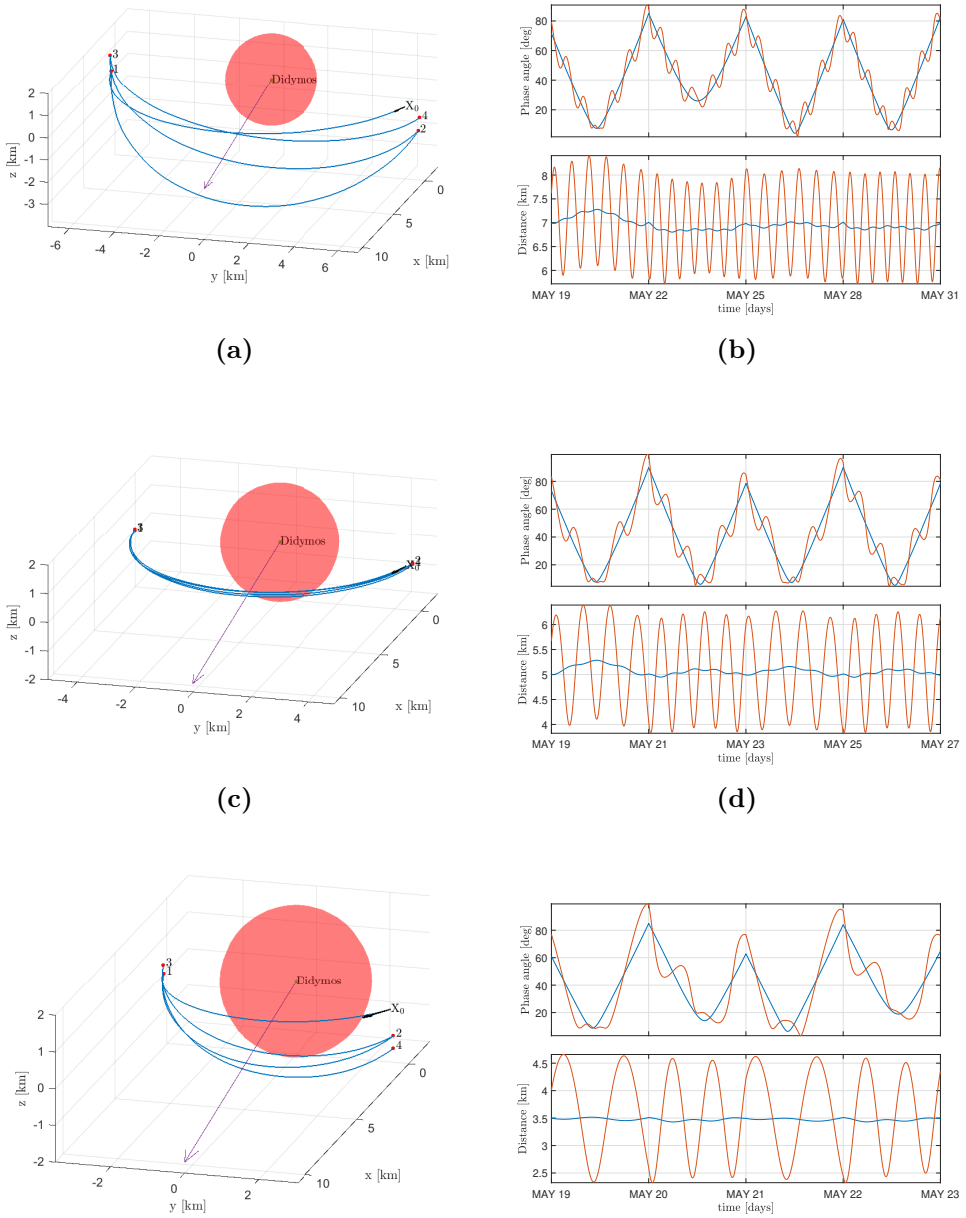

Figure 5.5: Quasi circular loop trajectories. a-b) Points at 7km, arc of 3 days. c-d) Points at 5km, arc of 2 days. e-f) Points at 3.5km, arc of 1 day. In purple the direction pointing the Sun. Next to the trajectories: the phase angle (Sun-asteroid-CubeSat) (up). The distance (down). In blue the data with respect to Didymain, in red the data with respect to Didymoon.

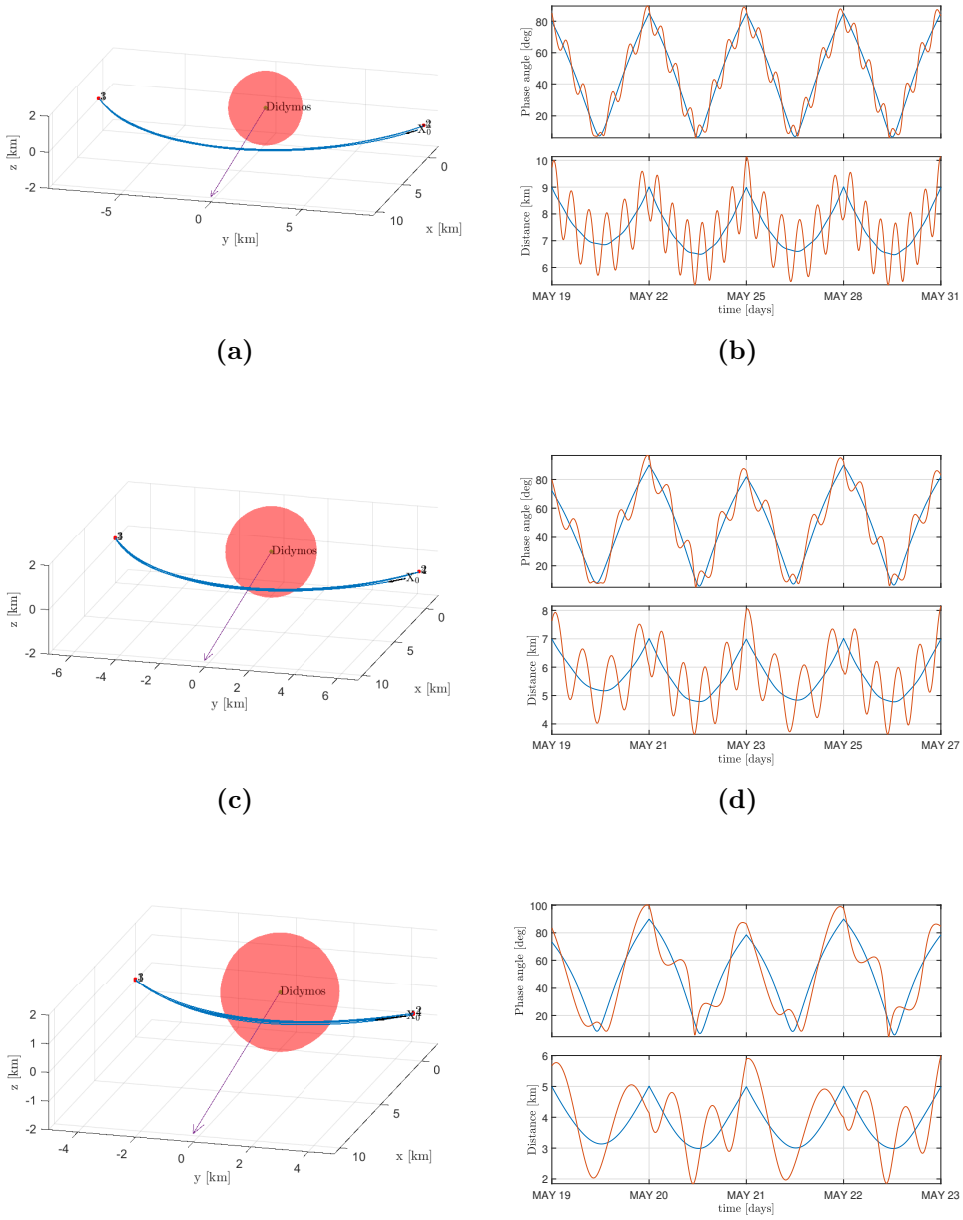

Figure 5.6: Loop trajectories with perigee at lower altitudes. a-b) Points at 9km, arc of 3 days. c-d) Points at 7km, arc of 2 days. e-f) Points at 5km, arc of 1 day. In purple the direction pointing the Sun. Next to the trajectories: the phase angle (Sun-asteroid-CubeSat) (up). The distance (down). In blue the data with respect to Didymain, in red the data with respect to Didymoon.

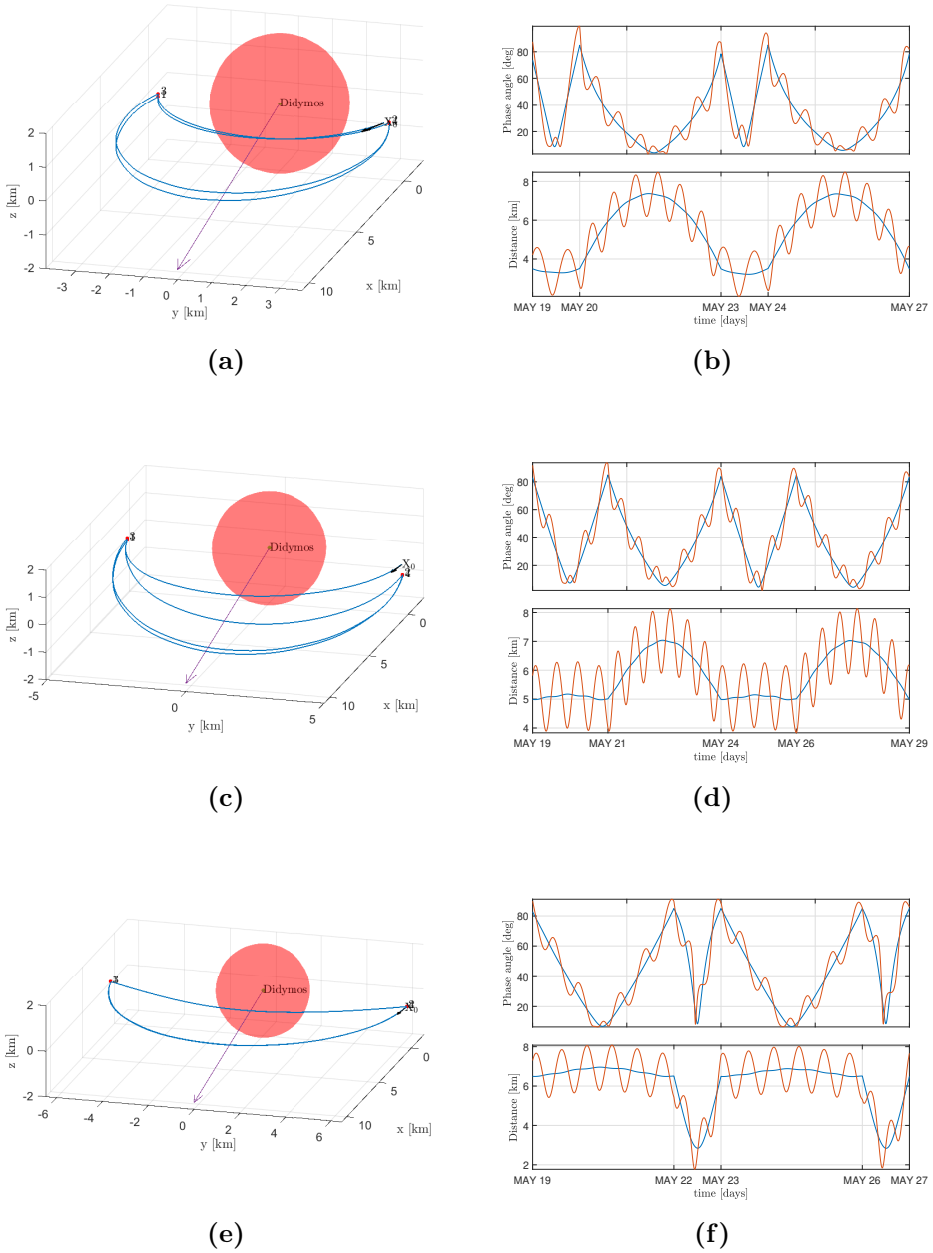

Figure 5.7: Peculiar loop trajectories with costumed maneuvers frequency. a-b) Points at 3.5km, maneuvers each 1 and 3 days. c-d) Points at 6.5km, maneuvers each 3 and 1 days. e-f) Points at 5km, maneuvers each 2 and 3 days. In purple the direction pointing the Sun. Next to the trajectories: the phase angle (Sun-asteroid-CubeSat) (up). The distance (down). In blue the data with respect to Didymain, in red the data with respect to Didymoon.

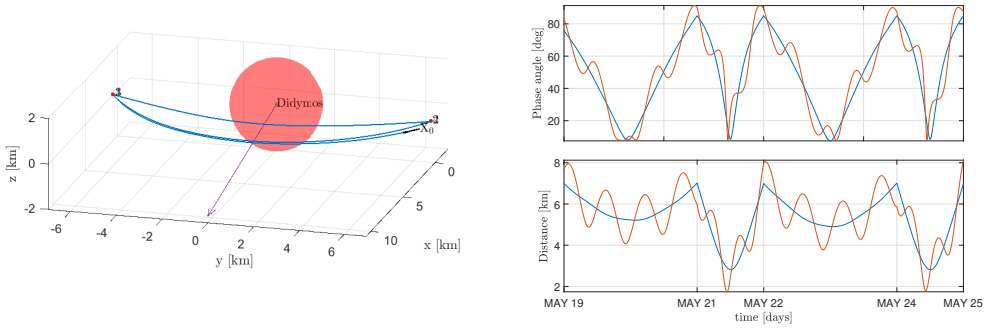

(a) **(b)**

Figure 5.8: Loop trajectories where the maneuver points are placed far from the asteroid. a-b) Points at 7km, maneuvers frequency each 2 and 1 days. In purple the direction pointing the Sun. Next to the trajectory: the phase angle (Sun-asteroid-CubeSat) (up). The distance (down). In blue the data with respect to Didymain, in red the data with respect to Didymoon.

ΔV_1	ΔV_2	ΔV_3
21.56	21.27	21.49

(a)
Cost of Fig. 5.7a

ΔV_1	ΔV_2	ΔV_3
18.23	18.21	18.27

(b)
Cost of Fig. 5.7c

ΔV_1	ΔV_2	ΔV_3
20.05	20.04	20.06

(c)
Cost of Fig. 5.7e

ΔV_1	ΔV_2	ΔV_3
22.90	23.02	23.04

(d)
Cost of Fig. 5.8a

Table 5.5: Cost of the peculiar loop maneuvers in cm/s

Fig. 5.6, Fig. 5.5 and Fig. 5.4 perfectly show the three operative regions anticipated before. As expected, the shortest the time to perform the arc, the closer the perigee. Excluding the trivial solutions of placing the maneuver points as close as possible, minimum distances of 6.5km, 5km and 3.5km can be obtained for maneuvers frequencies of 3, 2 and 1 day.
Wide variety of phase angles from few degrees up to 80° can be obtain in every operative regions. Fig. 5.7 shows the possibility to customize the maneuver frequency when more relaxed maneuver timetables or different performance between two consecutive arcs are needed.

5.2 Retrograde Equatorial trajectories

Retrograde equatorial orbits are known to be strongly stable against gravitational instabilities. These solutions have been widely used in past also around asteroids, as for Itokawa[38]. These features have been exploited by designing a three loop trajectory where the first two points are on the equator while the third is an intermediate point before returning to the initial position.
In this section, the design of the maneuver points for these retrograde equatorial orbits is shown. The trajectory degrees of freedom are highlighted and a grid search aimed to study the stability of the solutions as function of their degrees of freedom is described. Finally, some possible solutions are shown and commented.

Desired maneuver points design

This trajectory is composed by only three points. However, several trajectories can be combined to form a longer loop around Didymos.
The first two points are constrained to be on the equator at a desired altitude from Didymos and their azimuthal position around the asteroid is chosen by maximizing their distance such that the first arc is retrograde. Instead, the third point is chosen to be at the maximum distance from both the initial points. By doing that, it would be far from the equator ensuring the possibility of exploring high-declination regions.

Retrograde equatorial grid search

A grid search was conducted on the multiple combinations of degrees of freedom which are: the three different distances from the system barycenter of the three points involved and the duration of each parabolic arc. Initially, a constrained on the duration of each arc of 3 or 4 days have been requested. However, the possibility of performing two consecutive maneuvers after 2 days was also investigated. All the possible values of the chosen degrees of freedom are depicted in Table 5.6.

$\mathbf{X_1}$	2,3,4,5
$\mathbf{X_2}$	2,3,4,5
$\mathbf{X_3}$	2,3,4,5
$\mathbf{\Delta t_1, \Delta t_2, \Delta t_3}$	2,3,4

Table 5.6: Candidate distances from the system barycenter and durations of the parabolic arcs considered. Distances are expressed in km while duration in days.

Starting from the first arc, the boundary value problem for each consecutive pair of points is solved for all the time options. First a simple Newton's method is used as a correction strategy. Then, if the solution is not stable, a gradient descent algorithm is used for further control. At the end of each propagation, if the solution is not stable, it is discharged and no further integrations are done to continue from that point. Otherwise, if the solution is good, the algorithm continues to try all the possible combinations for the next parabolic arc. In the end, only the combinations of points and durations that have managed to survive until the return to the starting point can be considered eligible for a possible orbit. A graphical representation of how the algorithm works is shown in Fig. 5.9 while the results are shown in Fig. 5.9 and Table 5.5. The results are split in three images for clarity. The first represents the trajectories for a first arc of 2 days, the second for a first arc of 3 days and the third for a first arc of 4 days. From the stable triplets, some useful information can be retrieved. From Table 5.5, it is evident that a good option is to place the maneuver points at the same distance from the system barycenter. Copious stable solutions are present for maneuver points in this configuration, especially far from the asteroid, as expected. However, Table 5.5 can give also several solutions with triplets of points at different altitudes showing good stability properties in terms of number of possible combinations of arcs' durations.

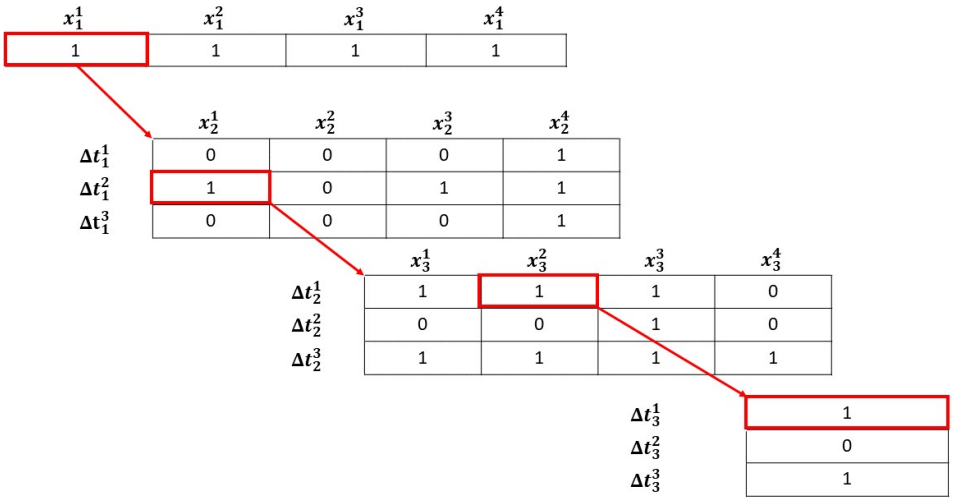

Figure 5.9: A graphic representation of how the algorithm works and how it highlights the right path. A good solution is marked with a 1 while a bad solution is marked with a 0. When a 1 appears, the algorithm proceeds to the next possible arcs. In the image it is highlighted the path followed to design the orbit passing through X_1^1-X_2^1-X_3^2-X_1^1 with maneuvers distant of Δt_1^2 - Δt_2^1 -Δt_3^1

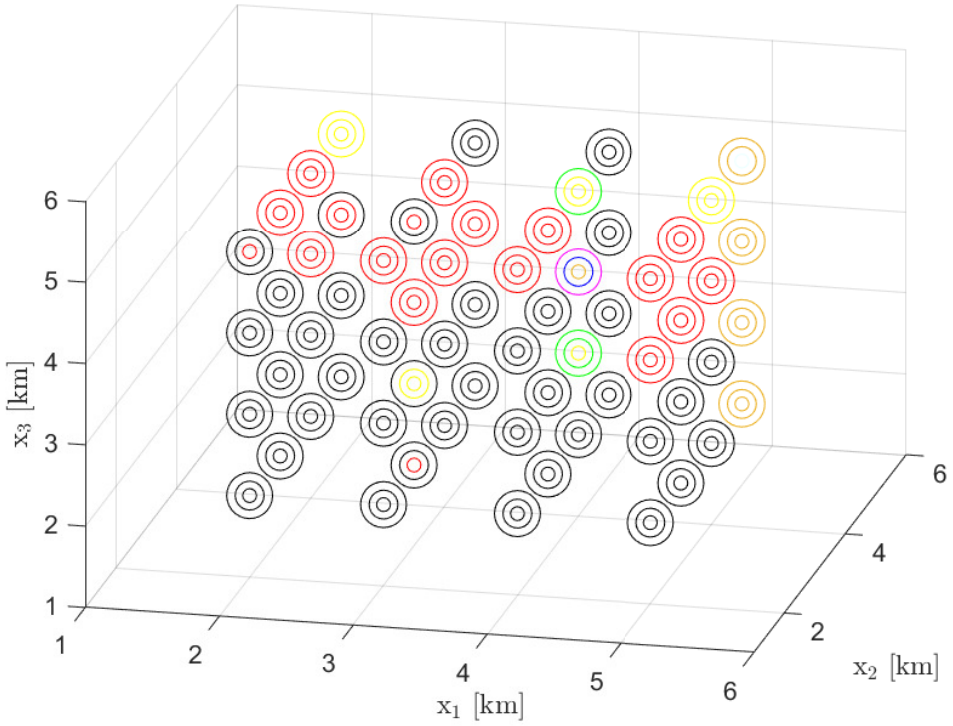
6
5
4
3
2
1
x3 [km]
1
2
3
4
5
6
x1 [km]
2
4
6
x2 [km]

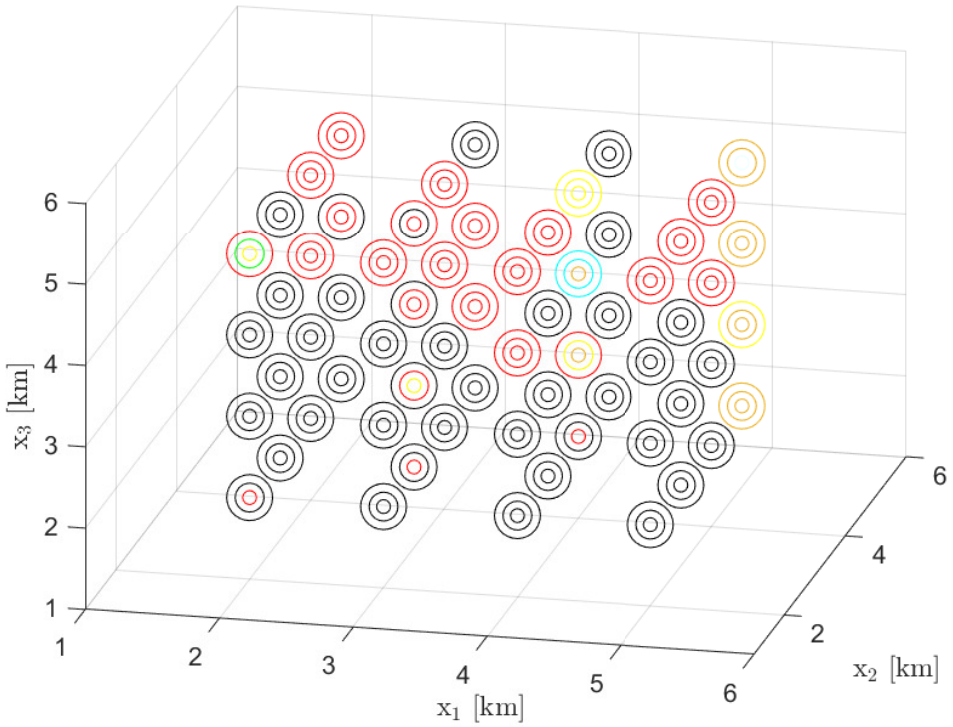
6
5
4
3
2
1
x3 [km]
1
2
3
4
5
6
x1 [km]
2
4
6
x2 [km]

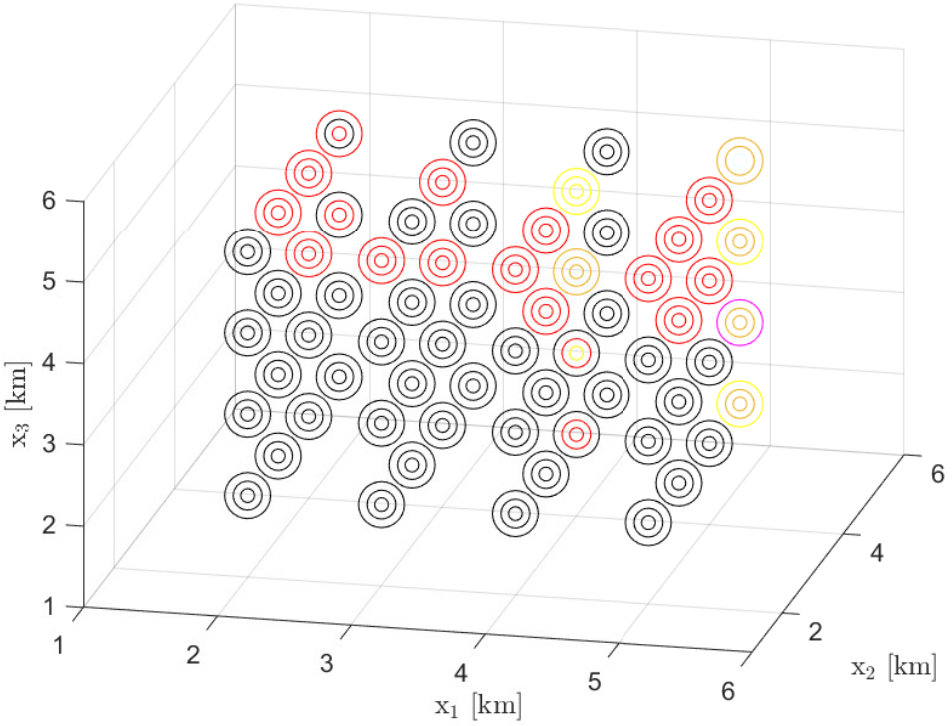

Figure 5.9: Stability results for $\Delta t_1 = 2$ days (up), for $\Delta t_1 = 3$ days (center) and for $\Delta t_1 = 4$ days (down). The solutions are shown as circles with different lengths and colours. The shape represents the duration of the third arc. From the smaller with $\Delta t_3 = 2$ days, to the bigger with $\Delta t_3 = 4$ days. Colours are for the second arc. Red, green and blue should be for trajectories admitting only a Δt_2 of 2, 3 and 4 days, respectively. Yellow circles are solutions admitting both a Δt_2 of 2 and 3 days. Magenta circles are for Δt_2 of 2 and 4 days, Cyan circles are for Δt_2 of 3 and 4 days, while gold circles are solutions in which all the durations considered are possible for the second arc. Black circles are unstable solutions.

Stable position triplets	Stable duration triplets
2,2,2	(3,2,2)
2,2,5	(2,2,2) (3,2,2) (3,2,4) (3,3,2) (3,3,3)
2,3,5	(2,2,2) (2,2,3) (4,2,2) (4,2,3) (4,2,4)
2,4,4	(2,2,2) (2,2,3) (2,2,4) (3,2,2) (3,2,3) (3,2,4) (4,2,2) (4,2,3) (4,2,4)
2,4,5	(2,2,2) (2,2,3) (2,2,4) (3,2,2) (3,2,3) (3,2,4) (4,2,2) (4,2,3) (4,2,4)
2,5,4	(2,2,2) (2,2,3) (3,2,2) (3,2,3) (4,2,2) (4,2,3)
2,5,5	(2,2,2) (2,2,3) (2,2,4) (2,3,2) (2,3,3) (2,3,4) (3,2,2) (3,2,3) (3,2,4) (4,2,2) (4,2,4)
3,2,5	(2,2,2) (2,2,3) (2,2,4) (3,2,2) (3,2,3) (3,2,4) (4,2,2) (4,2,3) (4,2,4)
3,3,2	(2,2,2) (3,3,2)
3,3,3	(2,2,2) (2,2,3) (2,3,2) (2,3,3) (3,2,2) (3,2,3) (3,3,2)
3,3,4	(2,2,2) (2,2,3) (2,2,4) (3,2,2) (3,2,3) (4,4,2)
3,3,5	(2,2,2) (3,2,2) (3,2,4)
3,4,4	(2,2,2) (2,2,3) (2,2,4) (3,2,2) (3,2,3) (3,2,4) (4,2,2), (4,2,3) (4,2,4)
3,4,5	(2,2,2) (2,2,3) (2,2,4) (3,2,2) (3,2,3) (3,2,4) (4,2,2) (4,2,3), (4,2,4)
3,5,3	(3,2,2) (3,2,3) (3,2,4)

Stable position triplets	Stable duration triplets
3,5,4	(2,2,2) (2,2,3) (2,2,4) (3,2,2) (3,2,3) (3,2,4)
4,2,4	(3,2,2) (3,2,3) (3,2,4)
4,2,5	(2,2,2) (2,2,3) (2,2,4) (3,2,2) (3,2,3) (3,2,4) (4,2,2) (4,2,3) (4,2,4)
4,3,4	(4,2,2) (4,2,3) (4,2,4)
4,3,5	(2,2,2) (2,2,3) (2,2,4) (3,2,2) (3,2,3) (3,2,4) (4,2,2) (4,2,3) (4,2,4)
4,4,2	(2,2,2) (4,2,2) (4,2,3)
4,4,3	(2,2,2) (2,3,2) (2,3,3) (2,3,4) (3,2,2) (3,2,3) (3,2,4) (3,3,2) (3,3,3) (3,4,2) (4,2,2) (4,2,3) (4,3,2)
4,4,4	(2,2,2) (2,2,4) (2,3,2) (2,4,2) (2,4,3) (2,4,4) (3,2,2) (3,3,2) (3,3,3) (3,3,4) (3,4,2) (3,4,3) (3,4,4) (4,2,2) (4,2,3) (4,2,4) (4,3,2) (4,3,3) (4,3,4) (4,4,2) (4,4,3) (4,4,4)
4,4,5	(2,2,2) (2,2,3) (2,3,2) (2,3,3) (2,3,4) (3,2,2) (3,2,3) (3,2,4) (3,3,2) (3,3,3) (3,3,4) (4,2,2) (4,2,3) (4,2,4) (4,3,2) (4,3,3) (4,3,4)
5,2,4	(2,2,2) (2,2,3) (2,2,4)
5,2,5	(2,2,2) (2,2,3) (2,2,4) (3,2,2) (3,2,3) (3,2,4) (4,2,2) (4,2,3) (4,2,4)

Stable position triplets	Stable duration triplets
5,3,4	(2,2,2) (2,2,3) (2,2,4) (4,2,2) (4,2,3) (4,2,4)
5,3,5	(2,2,2) (2,2,3) (2,2,4) (3,2,2) (3,2,3) (3,2,4) (4,2,2) (4,2,3) (4,2,4)
5,4,4	(2,2,2) (2,2,3) (2,2,4) (3,2,2) (3,2,3) (3,2,4) (4,2,2) (4,2,3) (4,2,4)
5,4,5	(2,2,2) (2,2,3) (2,2,4) (2,3,2) (2,3,3) (2,3,4) (3,2,2) (3,2,3) (3,2,4) (4,2,2) (4,2,3) (4,2,4)
5,5,2	(2,2,2) (2,2,3) (2,2,4) (2,3,2) (2,3,3) (2,3,4) (2,4,2) (2,4,3) (2,4,4) (3,2,2) (3,2,3) (3,2,4) (3,3,2) (3,3,3) (3,3,4) (3,4,2) (3,4,3) (3,4,4) (4,2,2) (4,2,3) (4,2,4) (4,3,2) (4,3,3) (4,3,4) (4,4,2) (4,4,3)
5,5,3	(2,2,2) (2,2,3) (2,2,4) (2,3,2) (2,3,3) (2,3,4) (2,4,2) (2,4,3) (2,4,4) (3,2,2) (3,2,3) (3,2,4) (3,3,2) (3,3,3) (3,3,4) (3,4,2) (3,4,3) (4,2,2) (4,2,3) (4,2,4) (4,3,2) (4,3,3) (4,4,2) (4,4,3) (4,4,4)
5,5,4	(2,2,2) (2,2,3) (2,2,4) (2,3,2) (2,3,3) (2,3,4) (2,4,2) (2,4,3) (2,4,4) (3,2,2) (3,2,3) (3,2,4) (3,3,2) (3,3,3) (3,3,4) (3,4,2) (3,4,3) (3,4,4) (4,2,2) (4,2,3) (4,2,4) (4,3,2) (4,3,3) (4,3,4) (4,4,2) (4,4,3)
5,5,5	(2,2,2) (2,2,3) (2,2,4) (2,3,2) (2,3,3) (2,3,4) (2,4,2) (2,4,3) (2,4,4) (3,2,2) (3,2,3) (3,2,4) (3,3,2) (3,3,3) (3,3,4) (3,4,2) (3,4,3) (3,4,4) (4,2,2) (4,2,3) (4,2,4) (4,3,2) (4,3,3) (4,3,4) (4,4,2) (4,4,3) (4,4,4)

Table 5.5: Stable retrograde equatorial loops: for each triplets of points' distances, the respective possible triplets of durations are listed. Distances are in km while durations in days.

Possible Retrograde Solutions

Here some possible solutions with retrograde arcs are shown.
Fig. 5.10 shows general solutions at different altitudes from the system.
Fig. 5.11 shows solutions with maneuver points at the same distance from the system. These trajectories are interesting not only for the variety of possible arcs' durations. Indeed, they can be easily repeated in a theoretical infinite loop to perform longer trajectories. Moreover, as in Fig. 5.11f, quasi-circular trajectories can be found with this configuration.
Fig. 5.12 shows particular solutions where 2 loops are combined to form a longer trajectory.
In Table 5.6 the maneuver costs for these trajectories are depicted.

ΔV_1	ΔV_2
20.95	10.32

(a)
Cost of Fig. 5.10a

ΔV_1	ΔV_2
13.31	12.86

(b)
Cost of Fig. 5.10c

ΔV_1	ΔV_2
28.35	21.40

(c)
Cost of Fig. 5.10e

ΔV_1	ΔV_2
16.93	20.99

(d)
Cost of Fig. 5.11a

ΔV_1	ΔV_2
14.50	15.57

(e)
Cost of Fig. 5.11c

ΔV_1	ΔV_2
12.06	10.82

(f)
Cost of Fig. 5.11e

ΔV_1	ΔV_2	ΔV_3	ΔV_4	ΔV_5
12.06	2.83	11.94	11.83	2.84

(g)
Cost of Fig. 5.12a

ΔV_1	ΔV_2	ΔV_3	ΔV_4	ΔV_5
14.67	18.45	18.72	14.10	15.45

(h)
Cost of Fig. 5.12c

ΔV_1	ΔV_2	ΔV_3	ΔV_4	ΔV_5
13.34	5.08	13.14	14.08	9.86

(i)
Cost of Fig. 5.12e

Table 5.6: Cost of the retrograde maneuvers in cm/s.

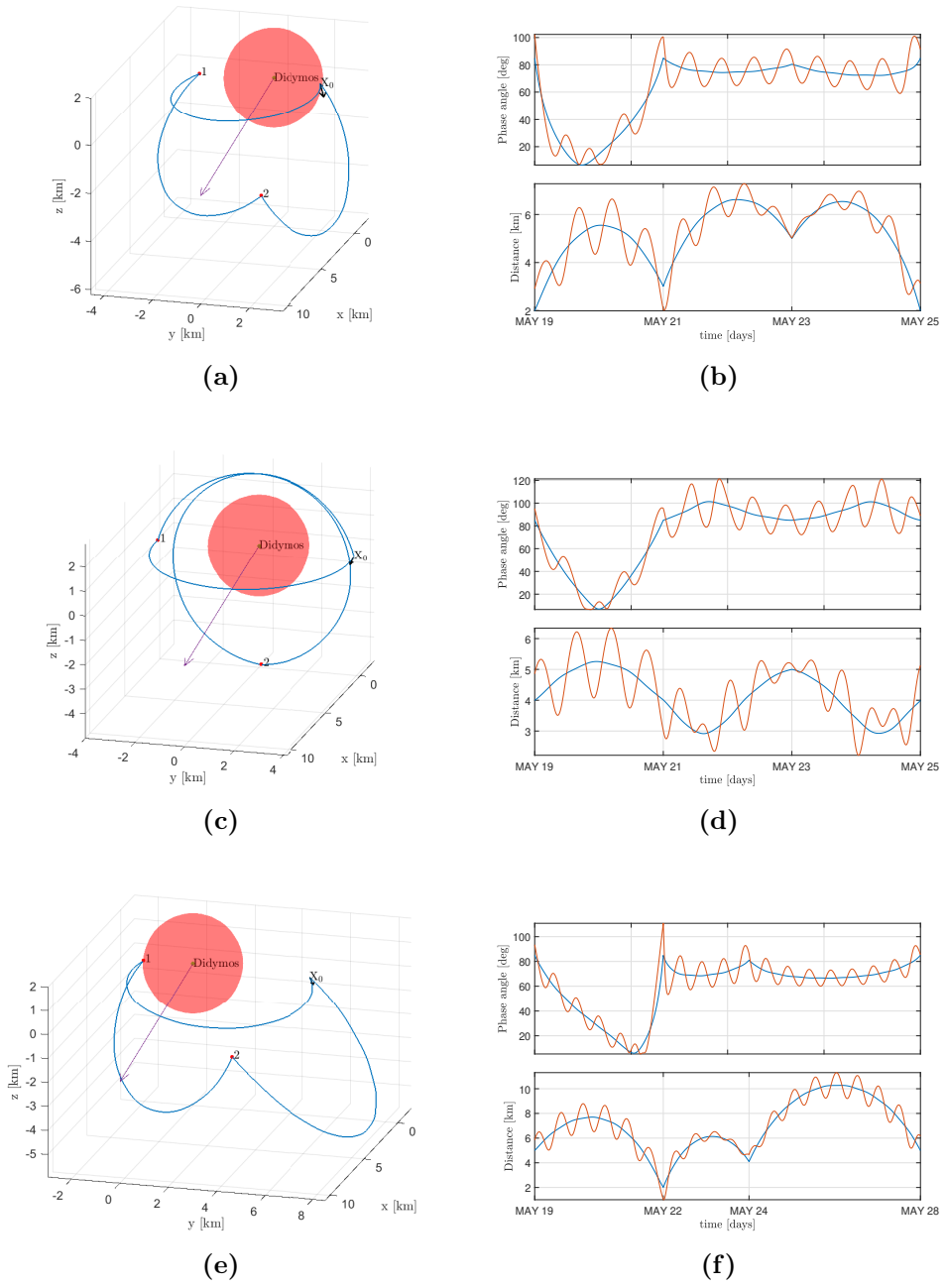

Figure 5.10: General retrograde equatorial trajectories. a-b) Points at 2-3-5km, arcs of 2-2-2 days. c-d) Points at 4-4-5km, arcs of 2-2-2 days. e-f) Points at 5-2-4km, arcs of 3-2-4 days. In purple the direction pointing the Sun. Next to the trajectories: the phase angle (Sun-asteroid-CubeSat) (up). The distance (down). In blue the data with respect to Didymain, in red the data with respect to Didymoon.

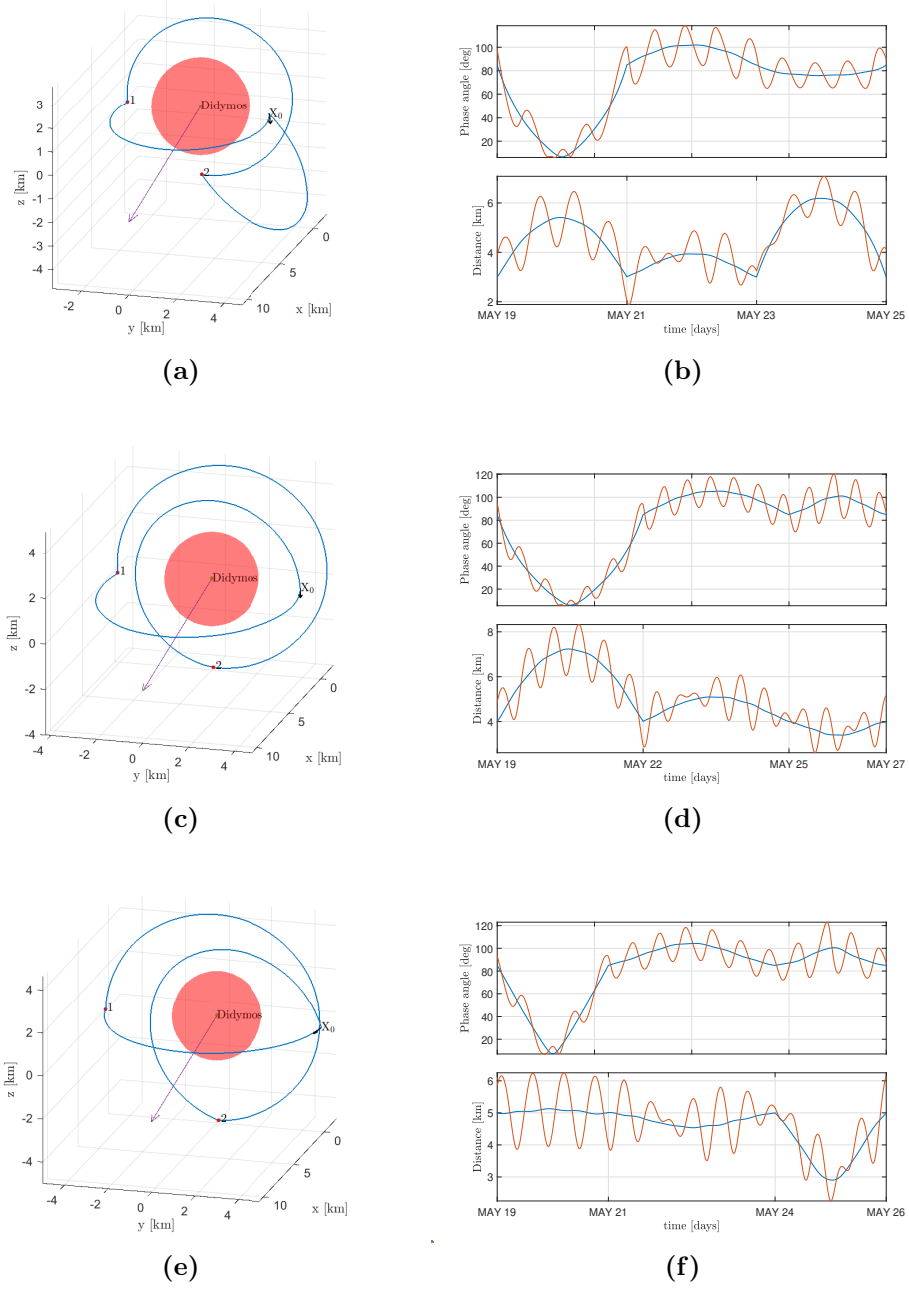

Figure 5.11: Retrograde equatorial trajectories with points at the same distance. a-b) Points at 3km, arcs of 2-2-2 days. c-d) Points at 4km, arcs of 3-3-3 days. e-f) Points at 5km, arcs of 2-3-2 days. In purple the direction pointing the Sun. Next to the trajectories: the phase angle (Sun-asteroid-CubeSat) (up). The distance (down). In blue the data with respect to Didymain, in red the data with respect to Didymoon.

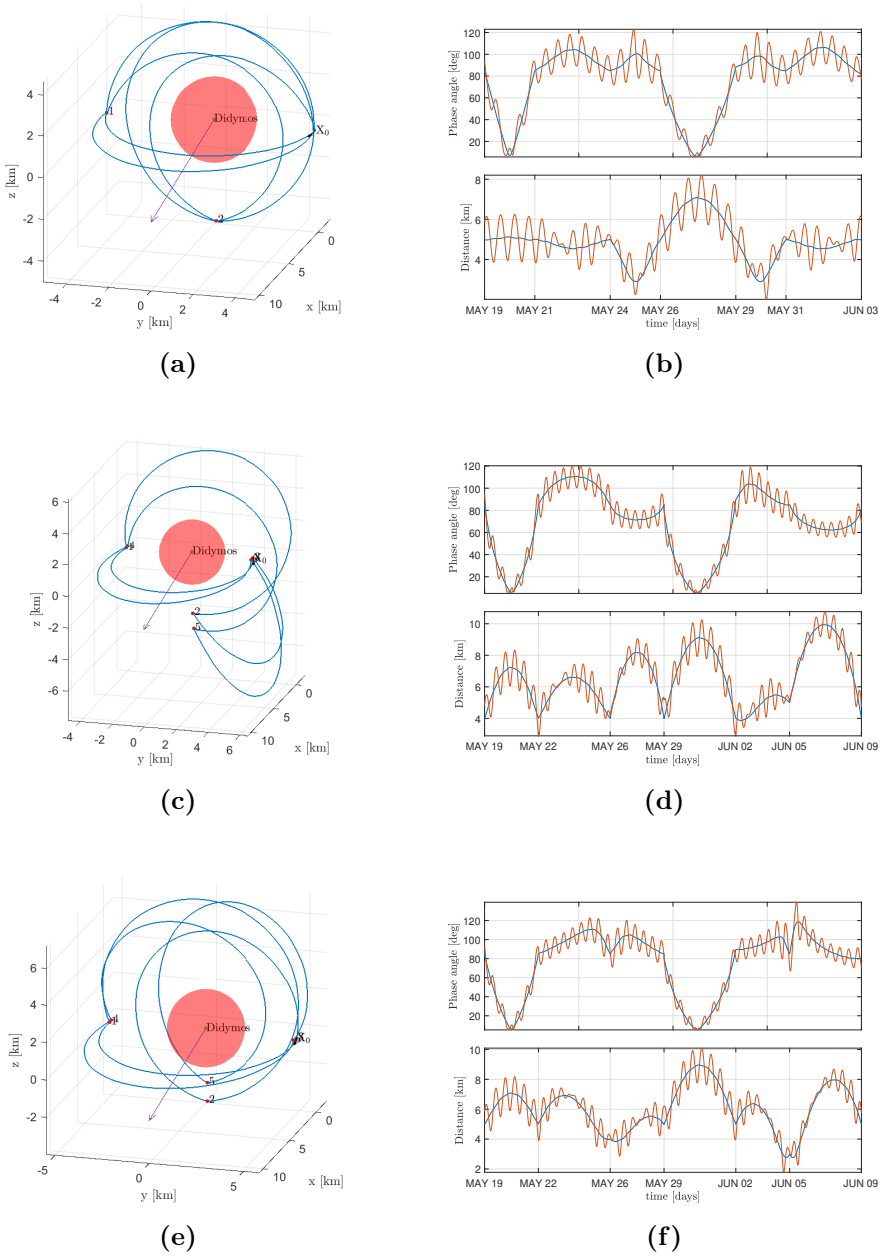

Figure 5.12: Combined retrograde equatorial trajectories. a-b) Points at 5-5-5-5-5-5km, maneuvers each 2 and 3 days. c-d) Points at 4-4-4-4-4-5km, maneuvers each 3 and 4 days. e-f) Points at 5-5-4-5-5-3km, maneuvers each 3 and 4 days. In purple the direction pointing the Sun. Next to the trajectories: the phase angle (Sun-asteroid-CubeSat) (up). The distance (down). In blue the data with respect to Didymain, in red the data with respect to Didymoon.

From Fig. 5.10, two retrograde equatorial loop solutions are visible. The former forms a shield shape which exhibits worse performance than loop cycle trajectories. Due to the additional constraint imposed on the declination of the first two points, the distance between them is less. Therefore, the minimum allowable altitude in the operative regions found in Section 5.1 is higher.
The other solutions consist of an initial retrograde equatorial arc and two quasi-Sun terminator orbit. The performance of the initial equatorial arc is still unsatisfactory with respect to the loop cycle solutions. However, the effectiveness of quasi-Sun terminator arcs is exceptional. The possibility of increasing the flight path and therefore the distance traveled between two consecutive points enables new operative regions in which lower altitudes can be reached with the same maneuver frequencies considered for the loop cycle. As seen in Fig. 5.10d, where, during an arc of 2 days between two points at 4km and 5km, a perigee of 3km is reached versus the 5km possible for a loop cycle. A similar behaviour is also present for maneuver points at the same distance in Fig. 5.11d. These arcs exhibit a peculiar behaviour of the distance from the system barycenter which does not reach its perigee/apogee in half the time of the ballistic arc.
As additional strength, these orbits can reach polar regions forbidden in the trajectories shown in Section 5.1, as clearly visible in all the figures in this section.
Fig. 5.12 shows the possibility of combining different three loop together to form longer trajectories. The main advantage of these configurations is to obtain orbits with maneuver frequency of 3 and 4 days that respect a weekly timetable useful from the point of view of ground control.

Chapter 6

Conclusions

This work deals with non-Keplerian proximity solutions around binary asteroids. The case study is the one of the NEA Didymos in the context of the AIDA mission. This chapter summarizes the results obtained after the investigation of the several aspects of the problem, together with a recall of the strategy pursued to achieve the desired goals.

The first objective was to study the dynamical environment close to the binary asteroid in a high fidelity model. In the past, as mentioned in Chapter 2, three-body-problems have been extensively studied in their circular approximation. However, to obtain an accurate dynamical description of the proximity of an asteroid, a general model of the effects is needed. Consequently, gravitational models different from the simple point-like one have been designed for the gravity field of the primaries. The gravitational perturbations of all the relevant massive bodies around the target have been considered, together with the not negligible effect of the Solar Radiation Pressure. As an additional element of accuracy, all the physical parameters and especially all the instantaneous positions of the celestial bodies considered were taken from the reliable ephemerides from ESA.
From the investigation, SRP and the solar gravity perturbation appeared to be the most important effects acting on a mass-less particle in proximity of the asteroid, together with the irregularities of the primaries' gravity field. At distances greater than 10 km, no high frequency variations of the gravity field are expected from Didymain's rotation around the system barycenter due to the proximity of his barycenter to it. While this is not true for Didymoon, the mass ratio between the primary asteroid and its moon is too small to let the latter influence the spectrum of the gravity field. During closer trajectories, such as those in Chapter 5, it may be possible to see the high frequency variations of the gravity field due to the effects of the F2BP, especially during quasi-circular orbits.

Concerning the second goal of comparing different gravity models and establishing a lower boundary for the point-like model, an expected result has been obtained. After an analysis of the point-like model's error obtained with respect to spherical harmonics and ellipsoid model, the former seems to be the most accurate. In fact, the ellipsoid shape model deviates from the point-like one closer to the asteroid, giving at the same altitude a lower error than spherical harmonics. However, since the mass ratio between the primary and its moon is high and Didymain's shape can be easily considered as quasi-spherical, the point-like model appears to be reliable up to 3 km from the system barycenter allowing for a maximum of 1% of error at 2.74 km.

Regarding the main purpose of this thesis to find proximity orbits around Didymos, important results have been obtained. The software built to find trajectories around the asteroid in the non-Keplerian environment of a R3BP can serve as a general purpose algorithm. After the setting of the dynamical environment, the software can find the correct orbit connecting two desired positions. Once a specific design has been chosen for the maneuver points, the algorithm corrects each initial state of the ballistic arcs needed to reach the next desired position. Then, grid search strategies were used to find possible stable solutions around the asteroid and a set of possible close trajectories have been collected.
For orbiting around Didymos, two different shapes have been considered. One made of a loop cycle near the equator, while the second is a three-points loop that can reach high declination values.

From the solutions in Section 5.1, a transition from hyperbolic to circular orbit was obtained. In particular, two different behaviour can be highlighted. The first where the maneuvers points are the closest points to the asteroid of the entire trajectory and the second where they are the farthest. Typically, the second configuration is preferred as scientific measurements away from maneuvers are promoted. As a boundary between these two, there is the possibility of performing circular orbits.
However, the two behaviours and their boundary share the position of the orbit perigee which seems to depend only on the flight time considered, together with the distance between the two maneuver points enforced in their design. As a result, different dynamical regions can be observed around Didymos. A perigee of minimum 6.5km can be obtained for a 3 days arc, while 5km can be obtained in 2 days and 3.5km in 1 day of flight.
Similar regions are expected to be observed by performing the same investigation to different binary systems due to the generality of the algorithms used.

Regarding the solutions in Section 5.2, searching for stable trajectories near the asteroid, interesting orbits were obtained. The three-loops found can be divided in two groups. The shield-shape trajectories do not exhibit interesting performance except for the possibility of reaching regions distant from the equator. Differently, the trajectories made by a retrograde equatorial arc and two quasi-Sun terminator orbits exhibit exceptional features. Because the spacecraft is forced to fly longer arcs, the minimum allowable altitudes are lower than those obtained in the loop cycle orbits. Although their design is not simple, since it seems impossible to force the Sun-terminator arc versus the shield-shape, these solutions can represent a step forward towards closer trajectories with maneuver frequency still in the order of days.
Particularly interesting is the possibility of performing combined loop with a frequency of 3 and 4 days in order to respect a weekly frequency of maneuvers' control that brings huge benefits from the ground operational point of view. In addition, during the same trajectory, both small and large phase angles are possible as the spacecraft orbits very distant regions of the asteroids during the loop.

List of Acronyms

Acronym	Meaning
AIDA	Asteroid Impact and Deflection Assessment
ARM	Asteroid Redirect Mission
ASPECT	Asteroid SPECTral imaging mission
AU	Astronomical Unit
CR3BP	Circular Restricted Three Body Problem
DART	Double Asteroid Redirection Test
ER3BP	Elliptical Restricted Three Body Problem
ESA	European Space Agency
F2BP	Full Two Body Problem
HF3BP	Hill Full Three Body Problem
JAXA	Japan Aerospace eXplloration Agency
LADEE	Lunar Atmosphere and Dust Environment Explorer
M-ARGO	Miniaturised – Asteroid Remote Geophysical Observer
NASA	National Aeronautics and Space Administration
NEA	Near Earth Asteroid
NEAR	Near Earth Asteroid Rendezvous
OSIRIS REx	Origins, Spectral, Interpretation, Resource, Identification, Security, Regolith Explorer
RHF4BP	Restricted Hill Full Four Body Problem
RF3BP	Restricted Full Three Body Problem
SRP	Solar Radiation Pressure
STM	State Transition Matrix

List of Symbols

Symbol	Meaning
a_H	Aphelion
p_H	Perihelion
a	Semi-major axis
e	Eccentricity
i	Inclination
T	Orbital period
n	Mean motion
a_{orb}	Distance between the center of the primary and the secondary
R_{g1}	Primary geometrical dimensions
R_{g2}	Secondary geometrical dimensions
M_1	Mass of the primary
M_2	Mass of the secondary
ρ_{bulk}	Assumed bulk density for both asteroids

Bibliography

[1] J. Veverka et al., *The landing of the near-shoemaker spacecraft on asteroid 433 eros*, Nature, 413:390–393, 2001.

[2] L. Hall, *"Lighten Up" - Deep Space Communications via Faraway Photons*, NASA Space Tech, 2017.

[3] R. Karimi, T. Martin-Mur, S. E. McCandless, *A Performance-Based Comparison of Deep-Space Navigation using Optical-Communication and Conventional Navigation Techniques: Small Body Missions*, AIAA SciTech Forum 2018 Space Flight Mechanics Meeting, 2018.

[4] M. Horányi et al., *The Lunar Dust Experiment (LDEX) Onboard the Lunar Atmosphere and Dust Environment Explorer (LADEE) Mission*, Space Sci Rev 185:93–113, 2014.

[5] T. Kubota et al., *Touchdown Dynamics for Sampling in Hayabusa Mission*, AIAA/AAS Astrodynamics Specialist Conference and Exhibit, 2006.

[6] T. Kominato et al., *Optical Hybrid Navigation and Station Keeping around Itokawa*, AIAA/AAS Astrodynamics Specialist Conference and Exhibit, 2006.

[7] Y. Tsuda et al., *System design of the Hayabusa2 — Asteroid sample return mission to 1999JU3*, Acta Astronautica 91:356–362, 2013.

[8] P. Muñoz et al., *Preparations and strategy for navigation during Rosetta Comet Phase*, Proceedings 23rd International Symposium on Space Flight Dynamics - 23rd ISSFD, 2012.

[9] U. Herfort, C. M. Casas, *Trajectory preparation for the approach of the spacecraft Rosetta to Comet 67P/Churyumov-Gerasimenko*, Proceedings 25th International Symposium on Space Flight Dynamics – 25th ISSFD, 2015.

[10] D. A. Lorenz et al., *Lessons learned from OSIRIS-REx autonomous navigation using natural feature tracking*, IEEE Aerospace Conference, 2017.

[11] D. R. Wibben et al., *Maneuver strategy for OSIRIS-REx proximity operations*, 10th International ESA conference on Guidance, Navigation and Control System, 2017.

[12] J. Gal-Edd, A. Cheuvront, *The OSIRIS-REx asteroid sample return mission operations design*, IEEE Aerospace Conference, 2015.

[13] N. Strange et al., *Overview of Mission Design for NASA Asteroid Redirect Robotic Mission Concept*, 33rd International Electric Propulsion Conference, 2013.

[14] R. Walker et al., *Miniaturised Asteroid Remote Geophysical Observer (M-ARGO): A stand-alone deep space CubeSat system for low cost science and exploration missions*, IPPW Small Sat Short Course, 2018.

[15] L. McNutt et al., *Near-Earth Asteroid Scout*, American Institute of Aeronautics and Astronautics Space Conference and Exposition, 2014.

[16] P. Michel et al., *European component of the AIDA mission to a binary asteroid: characterization and interpretation of the impact of the DART mission*, Advances in Space Research, 62:2261-2272, 2018.

[17] A. Pellacani et al., *HERA vision based GNC and autonomy*, 8th European Conference for Aeronautics and Space Sciences (EUCASS), 2019.

[18] H. R. Goldberg et al., *The Juventas CubeSat in Support of ESA's Hera Mission to the Asteroid Didymos*, 33rd Annual AIAA/USU Conference on Small Satellites, 2019.

[19] T. Kohout et al., *Feasibility of asteroid exploration using CubeSats — ASPECT case study*, Advances in Space Research, 62:2239-2244, 2017.

[20] J. Wahlund et al., *Asteroid Prospection Explorer (APEX) Cubesat For the ESA Hera Mission*, EPSC-DPS Joint Meeting 2019, 13:EPSC-DPS2019-1287-1, 2019.

[21] F. Dedori, *Politecnico e Agenzia spaziale europea: "Così difenderemo la terra dagli asteroidi"*, Il giorno, 2020.

[22] J. L. Margot et al., *Binary asteroids in the near-Earth object population*, Science, 296(5572):1445–1448, 2002.

[23] D. J. Scheeres, J. Bellerose, *The Restricted Hill Full 4-Body Problem: application to spacecraft motion around binary asteroids*, Dynamical Systems, 20(1):23-44, 2015.

[24] B. F. Villac, *Dynamics in the Hill problem with applications to spacecraft maneuvers*, University of Michigan, 2003.

[25] J. Bellerose, D. J. Scheeres, *Restricted Full Three Body Problem: Application to binary system 1999 KW4*, Journal of Guidance Control and Dynamics, 31(1):162-171, 2008.

[26] R. A. Werner, D. J. Scheeres, *Mutual potential of Homogeneous polyhedra*, Celestial Mechanics and Dynamical Astronomy, 91:337–349, 2005.

[27] D. J. Scheeres, *Stability of the planar full 2-body problem*, Celestial Mechanics and Dynamical Astronomy, 104:103–128, 2009.

[28] W. M. Kaula, *Theory of Satellite Geodesy*, Blaisdell, 1966.

[29] C. M. Roithmayr, *Contributions of Spherical Harmonics to Gravitational Moment*, AIAA Journal, 57(10):1-10, 2019.

[30] A. C. Mueller, *A Fast Recursive Algorithm For Calculating The Forces Due To The Geopotential*, NASA Johnson Space Center Internal Note No. 75-FM-42, 1975.

[31] F. Ferrari, *Non-keplerian models for mission analysis scenario about small solar system bodies*, Politecnico di Milano, 2016.

[32] D. J. Scheeres, *Dynamics about uniformly rotating ellipsoids: application to asteroids*, ICARUS 110:225-238, 1994.

[33] R. Werner, D. J. Scheeres, *Exterior gravitation of a polyhedron derived and compared with harmonic and mascon gravitation representations of asteroid 4769 Castalia*, Celestial Mechanics and Dynamical Astronomy, 65:313-344, 1997.

[34] I. Jeana, A. Ngb, A. K. Misraa, *Impact of solar radiation pressure modeling on orbital dynamics in the vicinity of binary asteroids*, Acta Astronautica, 165:167–183, 2019.

[35] A. Casadei, *An optical navigation filter simulator for a CubeSat mission to Didymos binary asteroid system*, Università di Bologna, 2018.

[36] K. Howell, *Three-dimensional periodic 'halo' orbits*, Celestial Mechanics, 32:53–71, 1984.

[37] J. Barzilai, J. M. Borwein, *Two-Point Step Size Gradient Methods* IMA Journal of Numerical Analysis, 8:141–148, 1988.

[38] G. Bellei, J. L. Cano, M. Sanchez, *Operational Orbiting Strategies About Minor Bodies*, 21st International Symposium on Space Flight, 2009.